Sigma J Eng Nat Sci, Vol. 44, No. 1, pp. 501–527, February, 2026

Sigma Journal of Engineering and Natural Sciences
Web page info: https://sigma.yildiz.edu.tr
DOI: 10.14744/sigma.2026.1995

Research Article

Comparative assessment of novel hooped and conventional Pelton wheel turbine runner using downcomer nozzles of different materials and exit diameter through experimental investigations

H. N. LAKDAWALA[1,2*], V. K. PATEL[2], G. C. CHAUDHARI[3], S. A. CHANNIWALA[4], T. R. PATEL[2]

[1]*Department of Mechanical Engineering, Dr. S. & S. S. Ghandhy Government Engineering College, Surat, Gujarat, 395007, India*
[2]*Department of Mechanical Engineering, Sardar Vallabhbhai National Institute of Technology, Surat, Gujarat 395007, India*
[3]*Department of Mechanical Engineering, C. K. Pithawala College of Engineering & Technology, Surat, Gujarat 395007, India*
[4]*Retired, Department of Mechanical Engineering, Sardar Vallabhbhai National University of Technology, Surat, Gujarat 395007, India*

ARTICLE INFO

Article history
Received: 02 October 2024
Revised: 12 November 2024
Accepted: 23 December 2024

Keywords:
Convergence Angle; Hooped Pelton Turbine Runner, Nozzles, Uncertainty Analysis; Variable Flow

ABSTRACT

Impulse turbines are significant because of their straightforward design and the lack of specialized expertise to create the runners. The hooped Pelton turbine runner with a 256 mm pitch circle diameter and a 40 mm hoop gap with a 4 mm hoop thickness was developed to reduce the bucket stress caused by water jets. The current paper investigates developed hooped and identical conventional Pelton turbine runners with a single downcomer nozzle of different sizes and materials to predict and compare performance parameters at variable flow conditions with uncertainty in measurements. In the present experimentation, two stainless steel nozzles of 17 mm and 23 mm and four polymeric material nozzles of 17mm, 18 mm,19 mm, and 23 mm were used for both runners. The nozzles have a range of convergence angles (24-32 degrees) and beta ratio (0.38 -0.49). The jet and velocity ratios of 11 to 15 and 0.362 to 0.492 were studied, respectively. The 17 mm stainless steel nozzle with conventional Pelton turbine runner combination has an 18.18% higher hydraulic performance than the hooped Pelton turbine runner under the full gate open condition. It was found that the runners experimented with 23 mm stainless steel nozzles gave maximum efficiency in the case of a hooped Pelton turbine compared to conventional runners at 20% gate opening. However, the polymeric nozzle was best for low runner speed, especially with the Hooped Pelton Turbine runner. The Hooped Pelton Turbine runner has exhibited excellent characteristics with less flow area (part gate opening) for the limited runner speed range than the Conventional Pelton Turbine runner and similar hydraulic characteristics to the conventional runner. Thus, the present study provides a maximum performance aspect of a hooped Pelton turbine runner for nozzle selection.

Cite this article as: Lakdawala HN, Patel VK, Chaudhari GC, Channiwala SA, Patel TR. Comparative assessment of novel hooped and conventional Pelton wheel turbine runner using downcomer nozzles of different materials and exit diameter through experimental investigations. Sigma J Eng Nat Sci 2026;44(1):501–527.

***Corresponding author.**
*E-mail address: hnlgecs@gmail.com

This paper was recommended for publication in revised form by Editor-in-Chief Ahmet Selim Dalkilic

Published by Yıldız Technical University Press, İstanbul, Turkey

GRAPHICAL ABSTRACT

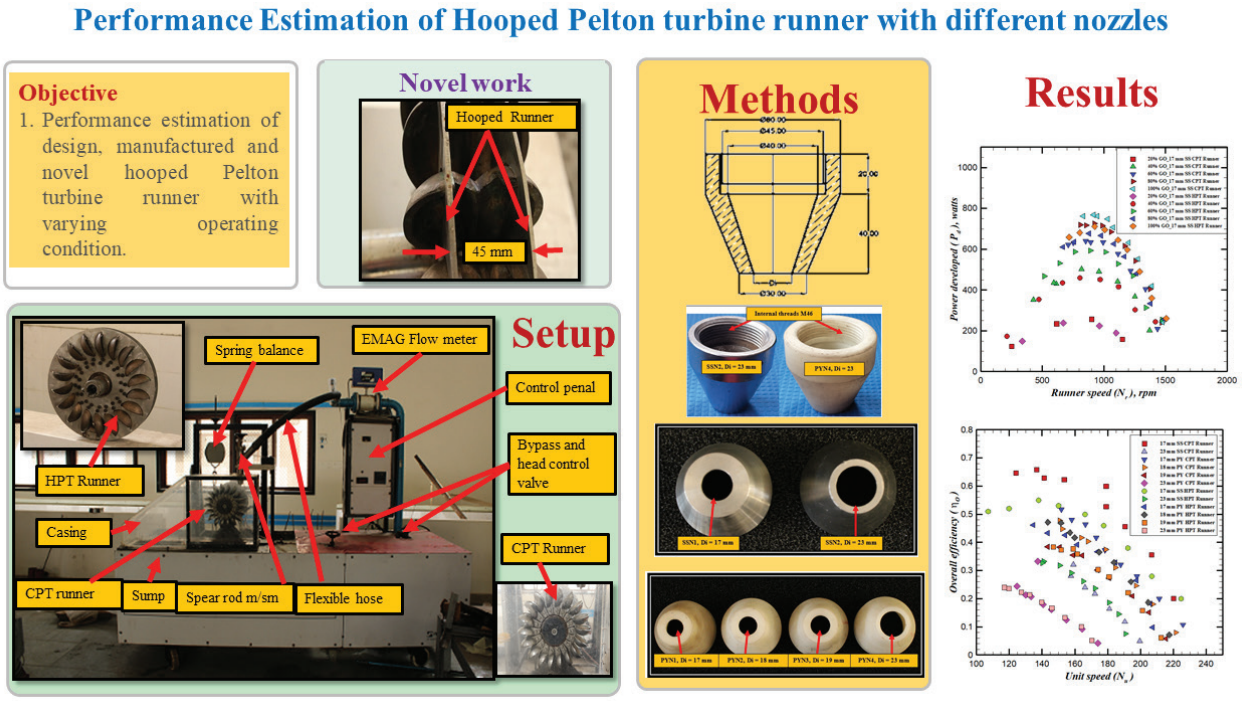

Highlights:

The following are the salient points for the present work

1. The newly developed Hooped Pelton Turbine Runner (HPT) was investigated for performance with different nozzles with the angle of convergence (Θ_n), jet ratio(m), and variable flow area.
2. The nozzle assembly's spearhead mechanism manually carries the flow variation.
3. The two stainless steel nozzles (SSN) and four polymeric material nozzles (PYN), identically sized, except for exit diameter and convergence angle (Θ_n), were used for the experimental investigations.
4. The comparative study also used the identically sized conventional Pelton turbine (CPT) runner.
5. The Hooped Pelton Turbine Runner (HPT) has shown excellent performance characteristics and stability under dynamic runner operation. The uncertainty analysis was conducted for 100 % gate opening (GO) and maximum hydraulic efficiency$(\eta h)_{max.}$

INTRODUCTION

Hydropower is considered the most valuable and sustainable source of energy generation among all available renewable sources. Off-grid and isolated places are the main uses for small and medium hydropower. The most significant value in impulse turbines can be found in their versatility and ease of use, especially in part-load situations. Numerous research-based elements and performance assessments in real and software-based evaluation techniques, such as experimental and numerical ones, have been examined to quantify the hydropower spectrum and demonstrate its adaptability.

Nozzle and Jet

The quality of the jet is an essential operating parameter for determining the hydraulic performance of an impulse turbine. The spray or jet characteristics are determined by the flow stability emerging from the orifice of a nozzle [1]. The discharge coefficient, velocity coefficient, and contraction coefficient of the nozzles are primarily independent of nozzle geometry [2]. The nozzle geometry has a pronounced effect on the sonic lines and discharge coefficients [3]. The strong secondary flows produced by bends or bifurcations in the Pelton turbine system's distributor alter the jet diameter's surface deformation, deviation, and dispersion, causing the jet core to shift away from the nozzle's axis [4]. The radial velocity gradient at the impingement stagnation points correlates with the free jet centreline velocity and half-radius at the exact axial location [5]. The shape of the water jet significantly influences the turbine losses, and the stator significantly influences the efficiency of the hydraulic machine [6]. The hydraulic loss in the pipe and nozzle parts is less than in the rotating buckets of available water energy [7]. The increased jet velocity reduces the force coefficient, showing that more energy is lost. Also, pressure distribution on the surface of the bucket is more evenly spread for circular jets than rectangular ones [8]. The jet shape significantly affects the flow and torque characteristics of the Pelton turbine runner [9]. Increasing the nozzle diameter leads to an increase in

water discharge and a decrease in water head, which leads to decreased Pelton turbine performance (torque, brake power, efficiency, and the range of rotational speed) [10].

Increasing the nozzle's length-to-diameter ratio eliminates the occurrence of hydraulic flips correlated to the jet's trajectory with the liquid/air momentum flux ratio at the nozzle's exit diameter [11]. The initial jet velocity profile and subsequent jet surface form are considerably influenced by the nozzle aspect ratio (L/d); nozzles operate best at convergence angles between 15° and 100° [12]. With increased nozzle throat angles, the flow power decreases, and the Pelton turbine efficiency is affected by increasing power loss [13]. Also, the increased jet exit angle has improved efficiency with part load and whole needle opening [14]. The free jet of Pelton nozzles decreases the exit angle for higher values of unit discharge; the leading cause of the losses is friction [15]. For 90° and 45° sharp-edged nozzles, the model can study the Reynolds number's effect on losses, and the flow separation causes[16]. The high-speed imaging found that the wind-induced jet breakup mode occurs at Reynolds numbers below 8,700, using Ohnesorge's theory[17]. An improved efficiency system can be designed by optimal annular nozzles with multiphase flows, appropriate flow models, computational fluid dynamics (CFD) simulations, and optimization algorithms [18]. A new nozzle design method for high-efficiency crossflow turbines increased the maximum efficiency [19]. The suspended sediment is crucial to Pelton turbine design, operation, and maintenance [20].

Bucket and Runner Design

The bucket design optimization simulates unsteady water film flow using a boundary-fitted grid (BFG) [21]. The regions of the bucket surface contribute the most to the torque, and the backside of the bucket, with Coanda interaction between the bucket cut-out area and the water jet [22]. The dynamic flow pattern of the free-surface sheet flow in the rotating bucket conforms to the dynamic energy efficiency (ηEB) and power efficiency (ηPB)[23]. Also, in the numerical turbine runner design optimization for maximum efficiency, NURBS polynomials and a relatively small number of control points are required with various design variable combinations [24]. A reference Pelton turbine bucket design using Non-Uniform Rational B-Splines Modeling (NURBS) was developed [25], and an unsteady CFD simulation approach for different bucket design optimization of the Pelton turbine runner was found effective [26]. Once designed, the optimized fabrication of Pelton turbine runners reduced the manufacturing time by 30% over the casted runner [27]. Pelton turbine runners have maximum pressure distribution at the bucket tip and runner Pitch Circle Diameter (PCD) [28]. The advantage of the hooped runner over the traditional one is that the stress is minimized and distributed more efficiently. Buckets for a newly designed runner with added backplates to support the buckets, subjected to bending moment on the back of both the hemispherical cups, have been reduced [29], and the bucket geometry influences Pelton's performance [30]. The flow visualization study of jet and bucket interaction in traditional and hooped Pelton turbine runners and reduced stresses as evaluated by finite element (FE) analysis [31,32]. Fatigue analysis of simple and advanced hoop Pelton turbine buckets; better design and operating performance of the Pelton turbine bucket with minimum corrosion and failures [33].

Performance Estimation

The operating head influences the rotating bucket, free surface sheet flow, and hydrodynamic performance of a Pelton turbine [23]. The hydraulic performance for the conventional and hooped Pelton turbine runners for variable flow conditions is in close agreement [34], and the optimized hoop thickness is required for maximum hydraulic performance [35]. The Pelton turbine's performance depends upon the jet's shape, size, and quality, as well as the shape of the bucket [36]. Combining the impeller of the Pelton turbine on the shaft of a high-pressure multistage pump used in seawater, the Reverse Osmosis (RO) desalination package yielded a decrease in input power [37]. The roughness of the bucket and the Reynolds number on the model are applied for global efficiency scale-up in actual plants [38]. The hybrid Eulerian-Lagrangian method to investigate bucket geometry's influence on Pelton turbine efficiency is proper [39,40]. A numerical flow analysis in a 2-jet Pelton turbine with a k-ω SST turbulent model has shown increased efficiency [41]. The gravity and surface tension affect the efficiency of accurate scale-up models [42], and the Euler particle tracking model has shown that erosion influences hydraulic characteristics [43]. Developing and evaluating numerical modeling tools of the complex unsteady free surface flow developed in the turbine is helpful for performance estimation [44]. The laboratory-scale tests on two impulse (Pelton and Turgo) turbines showed that the Turgo turbine is more efficient with a speed ratio of 0.46. The jet misalignment leads to a drop in efficiency [45]. The failure analysis of a Pelton turbine runner's CFD approach identified the critical points on the bucket zone neck, coinciding with the crack caused by tensile stress (Centrifugal force) and compression [46]. The Pelton turbine at full load and part load, along with numerical analysis and visualized flow pattern in the passages, showed good agreement [47]. The bamboo material is designed with a square nozzle to rotate the Pelton turbine runner, which can produce a higher speed than the round copper nozzle [48].

The Pelton-type impulse turbine can be applied to the seawater reverse osmosis (RO) energy recovery system [49]. The multiple parameters can yield the best results for energy systems by optimizing these operating parameters. Optimization algorithms like hybrid genetic algorithm and particle swarm optimization (GA-PSO) can be applied for the performance of stand-alone hybrid energy systems [50]. Artificial intelligence and digitization contribute to achieving clean and affordable energy [51]. Even exergetic performance analysis can compare oxy-combustion and conventional gas

turbine power cycles [52]. Model Predictive Control (MPC) in microturbine generation systems leads to higher adaptability, outputs precise adjustment, and suitable power flow for stand-alone operation [53]. The properties of synthetic polymers can be used in medicine apart from engineering applications [54]. The mechanical behavior of wind turbine blades improves with nanofluid-graphene and glass fiber in epoxy resin [55]. Blade materials like stainless steel, e-glass, epoxy, and gray cast iron are the best for domestic windmill applications[56]. Also, for marine-based applications, an optimized K-type propeller with lightweight aluminum material was found to be appropriate [57]. A mini venturi wind turbine can be used for domestic applications without affecting avians and reducing noise [58]. The huge whistling noise from the windmill gearbox may cause severe damage to the living organisms in the sea [59], and the spatial analysis determines the installation sites of wind power plants using models to reduce such damage [60]. Implementing the latest technology sensors saves maintenance costs caused by a drop in the wind turbine generator gearbox's thermal performance [61].

Research Gap

Few researchers have conducted the numerical study of the hooped Pelton turbine, but none have designed, manufactured, or experimented. The researchers tried to develop a newer bucket design to evaluate the performance of the Pelton turbine runner numerically and experimentally, but not the bucket-supporting mechanism. The low and medium head responses were restricted to small-scale or laboratory-scale setups. The experimental performance evaluation for the hooped Pelton turbine runner with different convergence ratios and metallic and nonmetallic material nozzles is uncovered in the present study. In the current experimentation, identically sized Hooped Pelton Turbine (HPT) runners and Conventional Pelton Turbine (CPT) runners were designed and tested for performance estimation and subsequent comparison.

Research Objective

The research objective for the current study is

- To find the hydraulic performance of CPT and HPT runners with variable flow conditions at constant head.
- To find hydraulic performance with the same material nozzles but different convergence angles.
- To compare the hydraulic efficiency of HPT and CPT runners for nozzles with different convergence angles.

EXPERIMENTAL SETUP

Setup Details

Hydro turbo machines are vital in fluid power engineering and sustainable power production through water energy. In the case of impulse-type hydro turbo machines, the amount of torque depends on jet exit conditions, the shape of the aperture, opening velocity, viscosity of the fluid, and surrounding air at the application where the jet is

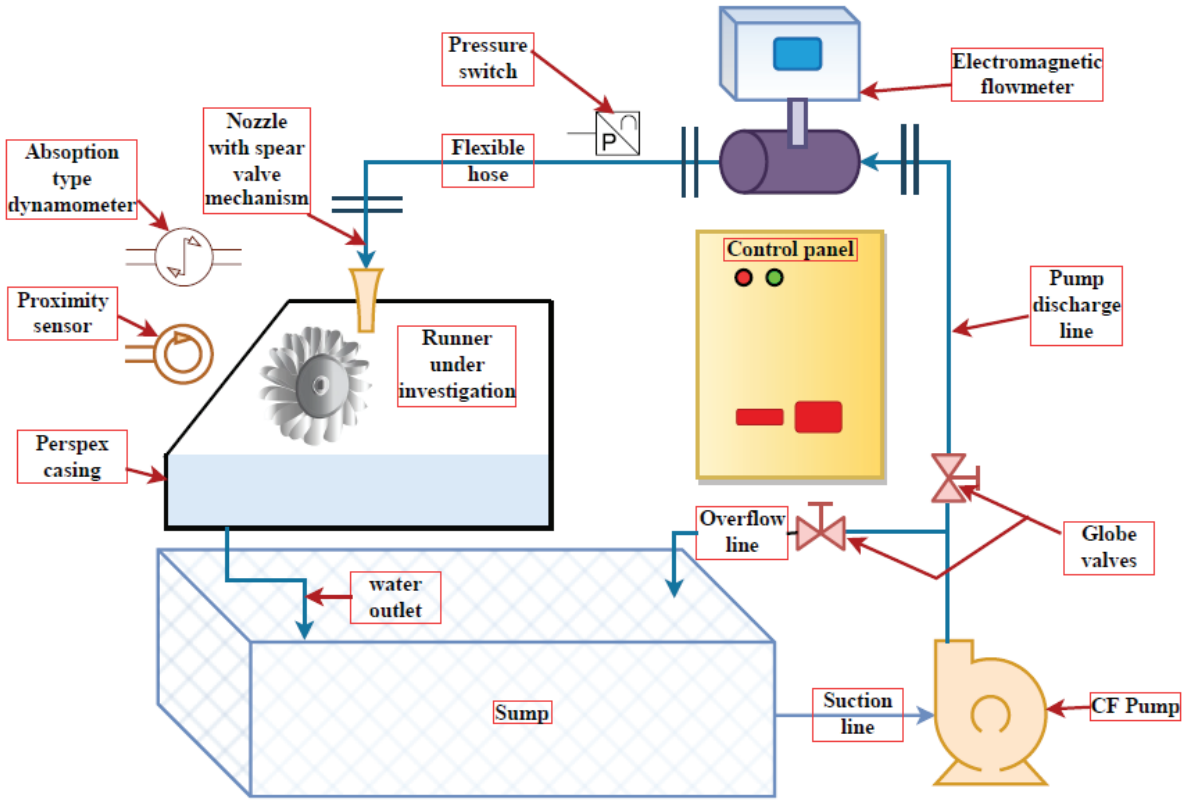

Figure 1. A line diagram -Experimental setup for testing impulse turbine runners.

employed. Since a jet is issued from the convergent nozzle of different sizes, research papers about such work are also cited. For conventional and hooped Pelton runners, relevant investigations are cited to clarify the work. The runners' design was carried out for maximum efficiency [62].

The head, flow conditions, and jet incidence variation significantly contribute to efficiency, torque characteristics, and turbine functioning points. A detailed evaluation of torque and thrust has shown that the cut-out and edge losses are the sources of loss in efficiency [63]. Numerical simulation showed that fiberglass-reinforced plastic for the bucket is better than cast iron under static conditions [64]. The parametric model of the bucket geometry, massive particle-based numerical simulations, and advanced optimization strategy can be used for the design optimization. Hence, the performance of a Pelton turbine runner increased [65]. The torque evolution and water sheet position for a revolving Pelton bucket simulation and the flow simulation of a stationary Pelton bucket using the finite volume particle approach for various impinging angles formed a new approach [66].

Figure 1 depicts the line diagram of the experimental setup used to examine two distinct runners for differing flow conditions, each with a different nozzle size and material. The setup,

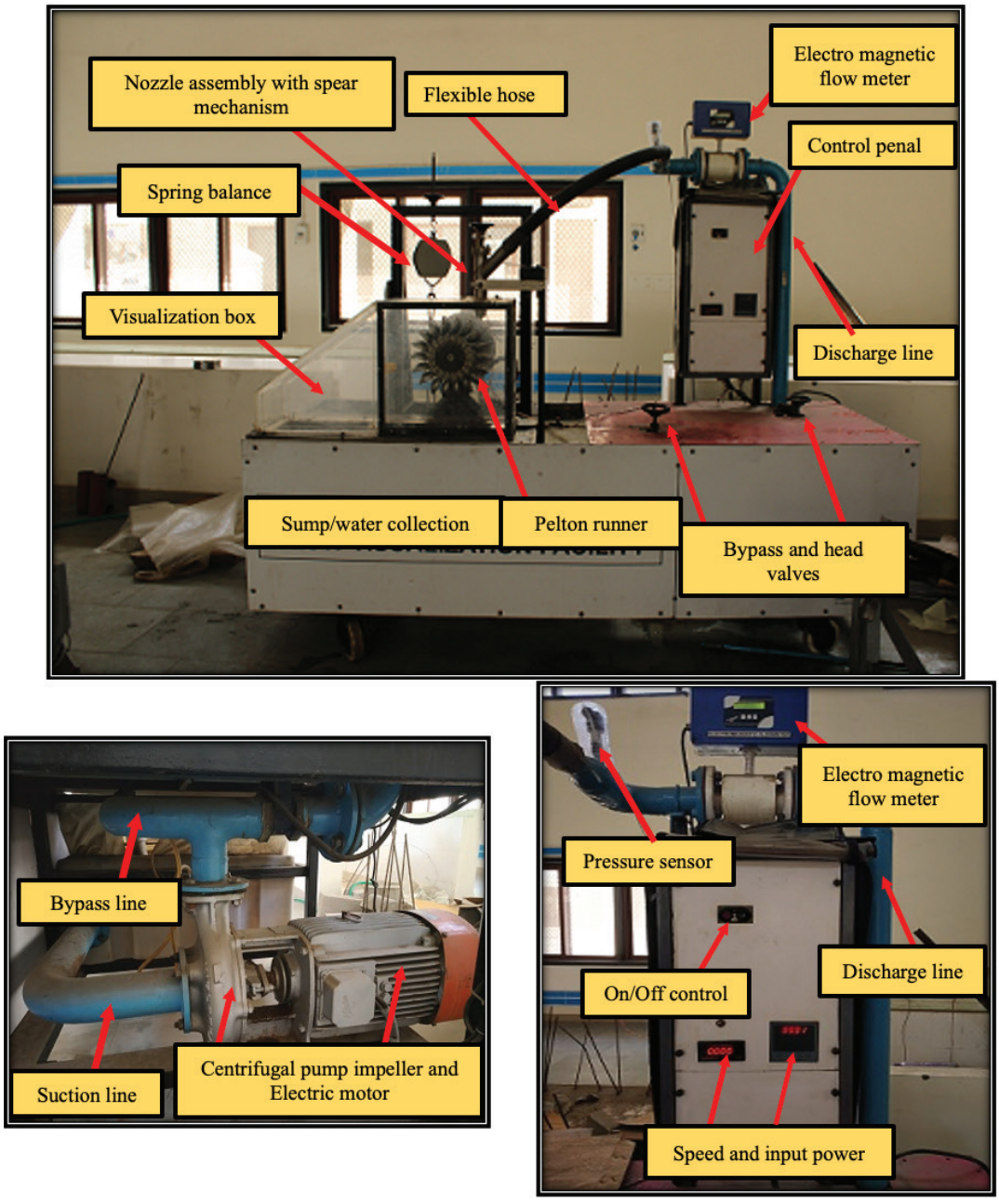

Figure 2. Experimental setup for Pelton wheel runners.

flow conditions, and experimentation approach are the same for both runners. The arrangement mentioned above comprises multiple parts, as indicated in Figure 2. A 5 HP electric pump motor (Kirloskar make) drives a strong flow rate through a line at the setup's sideways bottom, as seen in Figure 2. A 2.5-inch flow pipe transports the large water flow upward. It has a sizable centrifugal impeller to provide a straight flow through a flexible conduit. It comes with every fitting and valve required for the equipment to operate smoothly.

The discharge through the pump is measured using a line-mounted electromagnetic digital flow meter with a minimum flow measurement capacity of 0.00069 m^3/hr. The flow meter is lined up with polytetrafluoroethylene to provide a smooth passage for water flowing through it.

A flexible heavy hose is linked to the flow meter outlet and the main nozzle assembly to lessen the loss of piping length. The downcomer nozzle assembly's outer thread mounts and unmounts nozzles of different diameters and materials. A present study used two stainless steel (SSN) and four Polyacetal or Polyoxymethylene polymer (PYN) nozzles to evaluate the rotors' performance. The large rectangular sump at the bottom holds the water stream after striking the bucket and provides the opening for the Pump inlet to close the circuit of the test rig. The pressure sensor, model ADZ Nagano (Model SML-10,-1 - 25 bar,25 kg/cm^2), is kept after the flow meter to measure the pressure of fluid flowing through the pipe. The downcomer nozzle is fitted to a distance of less than 4Di to eliminate the possibility of jet spreading. A chamber comprises transparent acrylic sheets and digital still photography or movie shooting to enable flow visibility. The control panel has controls for starting and stopping the motor and a display for power input.

Investigated Variable Parameters

(a) Nozzle diameters

Figures 3, 4, and 5 depict the various nozzles used in the present study to investigate the main and operating characteristics of the Pelton turbine runners and then compare them [67]. The nozzle materials are selected as metallic and

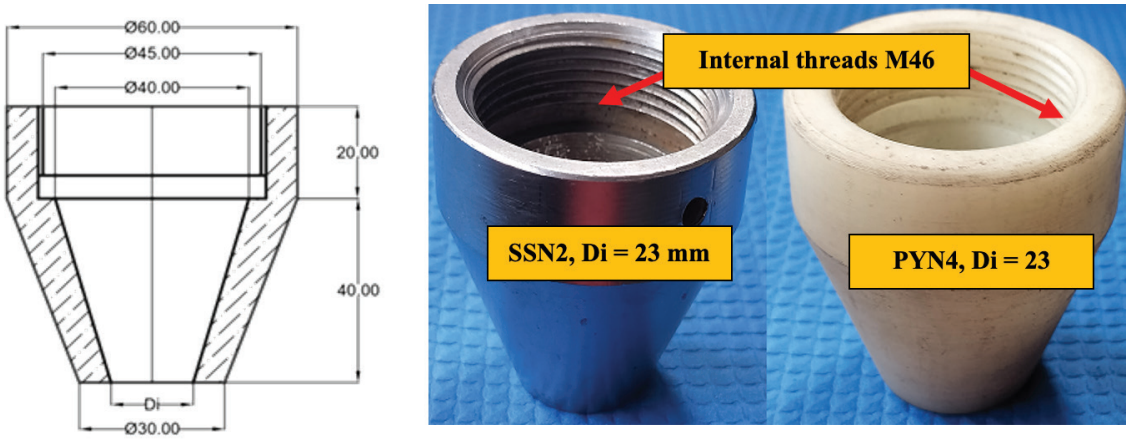

Figure 3. Cross-sectional view of the nozzle.

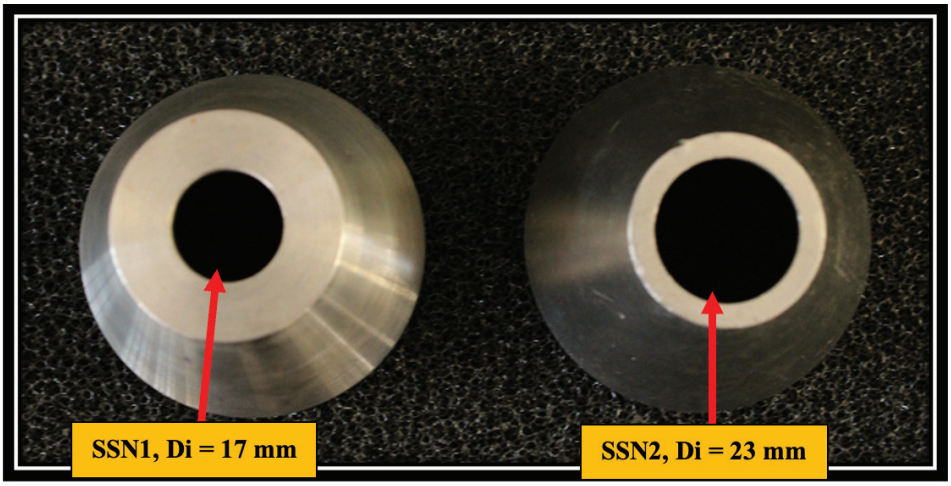

Figure 4. Stainless steel (SSN) nozzle top view left to right: a) D_i=17 mm, b) D_i=23 mm .

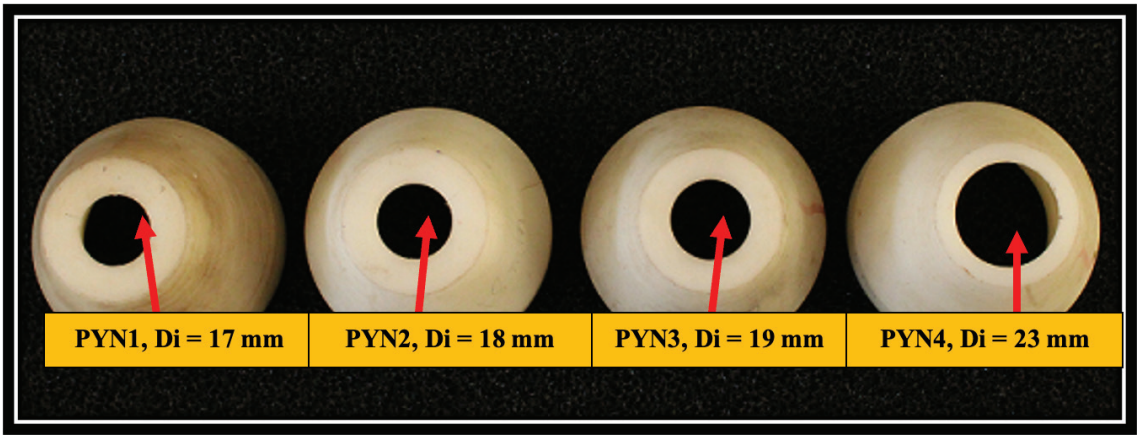

Figure 5. Polymer nozzle (PYN) top view a) D_i=17 mm b) D_i=18 mm c) D_i=19 mm d) D_i=23 mm.

Table 1. Geometrical parameters of the tested nozzles and material

Sr No.	Nozzle and its Specification	Size (Di), mm	Angle of convergence (Θ_n), Degrees	Beta ratio(β) (Di/Do)	Material of the nozzle
1	SSN1	17	32	0.38	Stainless steel (SS)
2	SSN2	23	24	0.49	Stainless steel (SS)
3	PYN1	17	32	0.38	Polyacetal or Polyoxymethylene
4	PYN2	18	30.5	0.40	Polyacetal or Polyoxymethylene
5	PYN3	19	29.5	0.42	Polyacetal or Polyoxymethylene
6	PYN4	23	24	0.49	Polyacetal or Polyoxymethylene

nonmetallic and have similar diameters. The length of the conical part is kept identical in all sets of nozzles at 40 mm, so the internal threading M 46 accommodates it on the nozzle-spear assembly.

As shown in Table 1 below, different materials and diameter nozzles are used for experimentation. For convenience, the code for each is depicted along with the specification. The cross-section of each of the mentioned nozzles is the same. Beta ratio (β) refers to the nozzle throat's diameter to the main pipe's diameter (D_i/D_o) range of 0.2 to 0.8 per ASME. Polyacetal is a lightweight material that provides less friction to fluid and is cheaper than stainless steel upon replacement. It is excellent in resisting many organic solvents, fuels, and weak acids, so it is suitable for varying water quality, including sediments.

In the present study, the dimensions and size of nozzles and runners employed are tabulated in Tables 1 and 2, respectively. The pipe with a 45 mm diameter and the nozzle inlet diameter of 40 mm are considered for beta ratio and convergence angle calculation, respectively. The nozzles have identical size and shape but differ in exit diameter and the resulting jet ratio. The angle of convergence and the beta ratio also differ. The material used for the above set of nozzles is different. The convergence angle for the nozzle depends on the inlet and exit diameters of the nozzles used. The maximum convergence angle in the present study is 32 degrees, with a beta ratio of 0.38 for 17 mm nozzles.

(b) Runner parameters

The Conventional and hooped Pelton turbine runners used for experimental investigation are shown in Figure 6. The geometric specifications for both runners are mentioned in Table 2. The runners are identical in construction and manufacturing except for the hooped plates. The buckets are bolted, and the internal surface of the bucket is polished to minimize friction losses. The runner disc and hub are integral parts and strong enough to cater to the load of all the buckets and hoop plates. The keyway in the hub matches the machine drum shaft keyway to accommodate the feather key. The hooped Pelton turbine runner is heavier than the Conventional Pelton turbine (CPT) runner. The hoop plates are bolted to the runner disc.

Table 2. Geometrical parameters of the tested runners

Sr No.	Description	Conventional Pelton Turbine (CPT)		Hooped Pelton Turbine (HPT)	
		Size (mm)	**Material**	**Size (mm)**	**Material**
1	**Bucket**		Stainless steel		Stainless steel
	Bucket width (W_b)	96 mm		96 mm	
	Bucket height (H_b)	90 mm		90 mm	
	Diameter to bucket width (D_p/W_b)	2.1		2.1	
	Number of buckets(Z)	18		18	
2	**Hub**		Stainless steel		Stainless steel
	Diameter of hub(d_{hub})	52 mm		52 mm	
	Length of the hub (l_{hub})	150 mm		150 mm	
	Size of keyway (Lx B)	10 x 5 mm		10 x 5 mm	
3	**Runner**		Cast steel		Cast steel
	The pitch circle diameter of the runner	256 mm		256 mm	
	Runner outside diameter	320 mm		320 mm	
	Runner width(r_b)	96 mm		96 mm	
4	Hoop thickness(h_t)	NA	----	4 mm	Stainless steel
5	Hoop gap(h_g)	NA	----	40 mm	----

A conventional Pelton turbine runner used for experimental investigation is depicted in Figure 6. It constitutes 18 double hemispherical buckets mounted on steel discs with the help of two stainless steel M12 bolts to complete the assembly. It has a central hole with a keyway to insert a feather key. A rubber padding is inserted on the front side and fastened with the help of bolts to prevent the axial movement of the runner. The inner surface of the bucket is made highly polished to reduce fluid friction losses upon gliding through the surface.

The hooped Pelton is an innovative new design based on the separation of function between buckets and hoops, as shown in Figure 6. The above figure also depicts the conventional Pelton Turbine runner used for investigation, along with the downcomer nozzle fitted tangentially at the top. This runner comprises separate buckets mechanically attached to a hub of two flanges (Hoops). The hoop plates are separated and located at a distance of 40 mm. The jet of fluid comes out from the bucket by gliding through the double hemispherical bucket surface, and to cater to this, notches are provided in the hoop plates. The novel hooped Pelton turbine runner has an excellent maintenance advantage and improved mechanical characteristics.

(c) Gate opening (variable flow area)

The gate opening in the present study for the variable flow area in all the nozzle runner combinations was carried

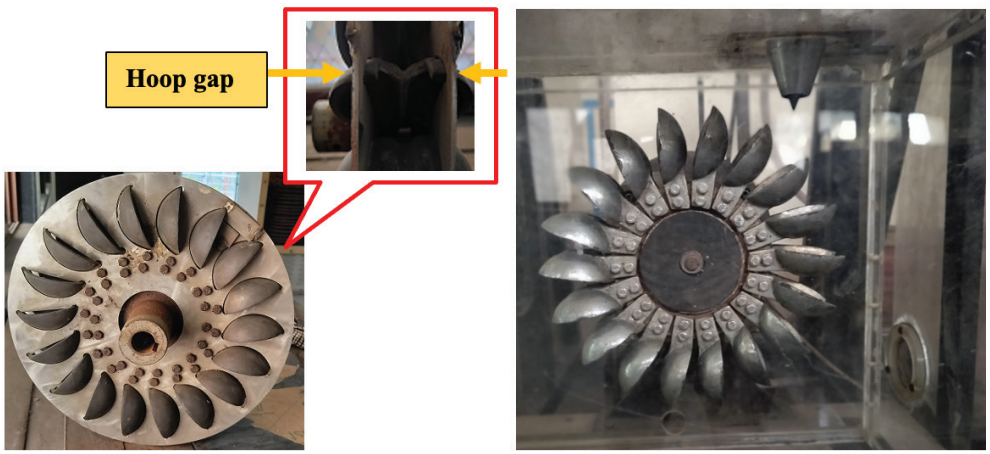

Figure 6. Hooped and conventional Pelton turbine runner (Left to right) under investigation.

out. The spear rod mechanism moves in and out to change the flow area based on the annular space between the spear rod and the tapered nozzle wall. In the present study, gate openings from 20 percent to 100 percent of the total flow area are taken during investigations.

MATERIALS AND METHODS

The parameters studied here include the flow interaction between the jet and rotating buckets in the turbine with variable flow area, convergence angle, and the jet ratio. The electromagnetic flow meter, weight, and spring balance are kept to observe various parameters. The experimental investigations were carried out continuously by changing the nozzles of various diameters. The head of water, 43 m, was maintained constant throughout the experimentation.

The calculation here leads to the various parameters like jet ratio (m) and velocity ratio/speed ratio (ϕ), the essential parts to describe the design and performance of the Pelton wheel turbine. The assumption is generally that the speed ratio's value is in the range of 0.42-0.48, and that of the jet ratio (m) changes from 10-18. In the present study, using a range of different diameter nozzles, the values are in the standard prescribed range. Table 3 below shows values obtained after the experiments.

The parameters were measured with various measuring devices and sensors. The present study takes care of the digital instruments with a digital display of the vital measured quantities like input power, runner speed, flow rate, and line pressure. Table 4 below states such parameters and corresponding measurements.

DATA REDUCTION

The various parameters like runner speed (Nr), dead weight (W), Spring balance reading (S), Power input (Pi), and Flow rate (Q) are observed and measured during experiments in the present study. The various quantities, like Hydraulic efficiency (ηh), Overall efficiency (ηo), the power developed (Pd), and torque available at the shaft (T) for all nozzle runner combinations, were estimated using the following equations.

$$N_s = N \frac{\sqrt{P_d}}{H^{\frac{5}{4}}} \quad (1)$$

Table 3. Jet ratio and velocity ratio at full gate opening (100 % GO)

Sr. No.	Nozzle	Size (mm)	Jet ratio (m=Di/Dp)	Velocity ratio ϕ (= u/Vjet)	
				Conventional Pelton Turbine (CPT) Runner	Hooped Pelton Turbine (HPT) Runner
1	SSN1	17	15	0.423	0.427
2	SSN2	23	11	0.492	0.436
3	PYN1	17	15	0.470	0.417
4	PYN2	18	14	0.466	0.444
5	PYN3	19	13	0.444	0.454
6	PYN4	23	11	0.425	0.362

Table 4. Measured parameters and corresponding instrumentation

Sr. No.	Parameters	Notation	Measurement
1	Input Power, kW	Pi	Motor power Sensors for voltage and current
2	Spring balance reading, kg	S	Subh, Accuracy class IV, 1 - 25 kg, 0.1 kg LC
3	Deadweight, kg	W	Cast iron counter slotted weight of known mass (set of 1 kg and 2 kg)
4	Runner speed, rpm	Nr	NPN-type revolution counter 2-20 mm, IP67, 10 to 30 VDC
5	Flow rate, m^3/hr	Q	Flowtech, Electromagnetic (MAG) Flowmeter, ± 1%, SS316, ±0.5% FSD, 0.3 to 10 m/s, 25 kg/cm^2
6	Percentage gate opening	%ge GO	Manually rotating the wheel in and out, the thread count
7	Pressure measurement, bar	p_g	ADZ Nagano SML-10, Electronic, SS304, ≤0.5% FSD,-1 - 25 bar, IP65, ceramic,4- 20 mA,12 to 32 V

$$N_s = \frac{\omega\sqrt{P_d}}{\sqrt{\rho}\left(gH\right)^{\frac{5}{4}}} \quad (2)$$

The dimensional and non-dimensional-specific speeds were found using Equations (1) and (2).

The power developed P_d on the shaft is expressed in kilowatts; the head H is expressed in m, and the speed ω is expressed in rad/s for Equation (1), and the power P_d is expressed in watts; the head H is expressed in m; the runner speed ω is expressed in rad/s; the density ρ is expressed in Kg/m^3 for Equation (2), respectively.

The unit quantities like unit power (P_u), Unit discharge (Q_u), and Unit speed (N_u) were evaluated using the formula given in Equation (3).

$$P_u = \frac{P_d}{H^{3/2}}, \quad Q_u = \frac{Q}{\sqrt{H}}, \quad N_u = \frac{N_r}{\sqrt{H}} \quad (3)$$

The torque developed on the runner is given by Equation (4)

$$T = \frac{\left(W - S\right) \times D_e \times g}{2} \quad (4)$$

The angular velocity of the runner, ω in terms of rad/s, was evaluated using Equation (5)

$$\omega = \frac{2\pi N_r}{60} \quad (5)$$

Mechanical power developed on the turbine shaft (P_d) was evaluated using Equation (6)

$$P_d = T \times \omega \quad (6)$$

Hydraulic efficiency(η_h) was evaluated using Equation (7)

$$\eta_h = \frac{P_d}{P_{in}} \times 100 \quad (7)$$

Where,

N_r = Speed of runner, rpm, P_{in} = Water power supplied to runner, Watt, W = Dead weight, kg, S= Spring balance reading , kg, D_e = Effective diameter of drum, m.

RESULTS AND DISCUSSION

The runners exhibited different performance characteristics with a nozzle combination and varying flow conditions under the constant head. The dynamic performance of Pelton turbines focuses on energy and power efficiency, discharge efficiency, and factors affecting performance under varying unit speeds [68,69]. The Conventional Pelton Turbine (CPT) and Hooped Pelton Turbine (HPT) runners were tested with all the nozzles and all the variable flow area situations.

Variation with Percentage Gate Opening for Different Nozzle Runner Combinations

The experiments were carried out with different nozzles and runners by restricting the flow area in percentage. The 17 mm SS nozzle (SSN1) characteristics for both runners are given in Figure 7. Both runners were found to have low torque in the range of 200 to 1200 rpm, with 80 % flow area restricted. The torque developed with a Conventional Pelton Runner shaft at 100% gate opening (GO) was about 9 N-m with 1000 rpm of the CPT runner. The least was found with a decrease in flow area (20% gate opening) in the case of both runners. The range over which power developed by the Hooped Pelton Turbine (HPT) runner with the 17 mm SS nozzle (SSN1) is found to be 700-1500 rpm, wherein maximum power is developed around 900 rpm.

The presence of two hooped steel plates 4 mm thick made the runner bulkier, so with the Hooped Pelton Turbine (HPT) runner, the values are identical at the higher runner speed, but the curve gets separated at the lower runner speed. The high unit discharge was found with the Conventional Pelton Turbine (CPT) runner compared to the Hooped Pelton Turbine (HPT) runner. The range of unit discharge for a conventional Pelton turbine (CPT) is more significant with unit speed than that of a hopped Pelton turbine (HPT). The unit discharge remains in the range of 1 to 1.5 for the most flow area variation corresponding to the range of unit speeds.

Figure 7 shows the operating parameter for a 17 mm stainless steel nozzle (SSN1) with a beta ratio of 0.38. The 17 mm exit diameter SS nozzle (SSN1) gave better efficiency and variation of parameters with runner speed and unit speed than any other combination used in the experimental study. The range of points and corresponding curves obtained with a 17 mm SS nozzle (SSN1)-Hooped Pelton turbine (HPT) runner are similar to standard curves for the Conventional Pelton turbine (CPT) runner. The power developed at the turbine shaft with a 17 mm SS nozzle (SSN1)- CPT runner combination is more than any other. The hydraulic efficiency obtained was higher with a 20% gate opening in the case of the CPT runner compared to the HPT runner for a 200 to 1000 rpm runner.

Figure 8 shows the variation of the main and operating parameters, including runner speed and unit speed, caused by using 23 mm stainless steel (SSN2). The 20 % gate opening variation dominates the Hooped Pelton turbine (HPT) runner. The maximum value of unit discharge is found with 100% gate opening in the case of the HPT runner. The nozzle with exit diameter (Di) used here is 23 mm of stainless steel (SSN2), with the highest beta ratio of 0.49, and

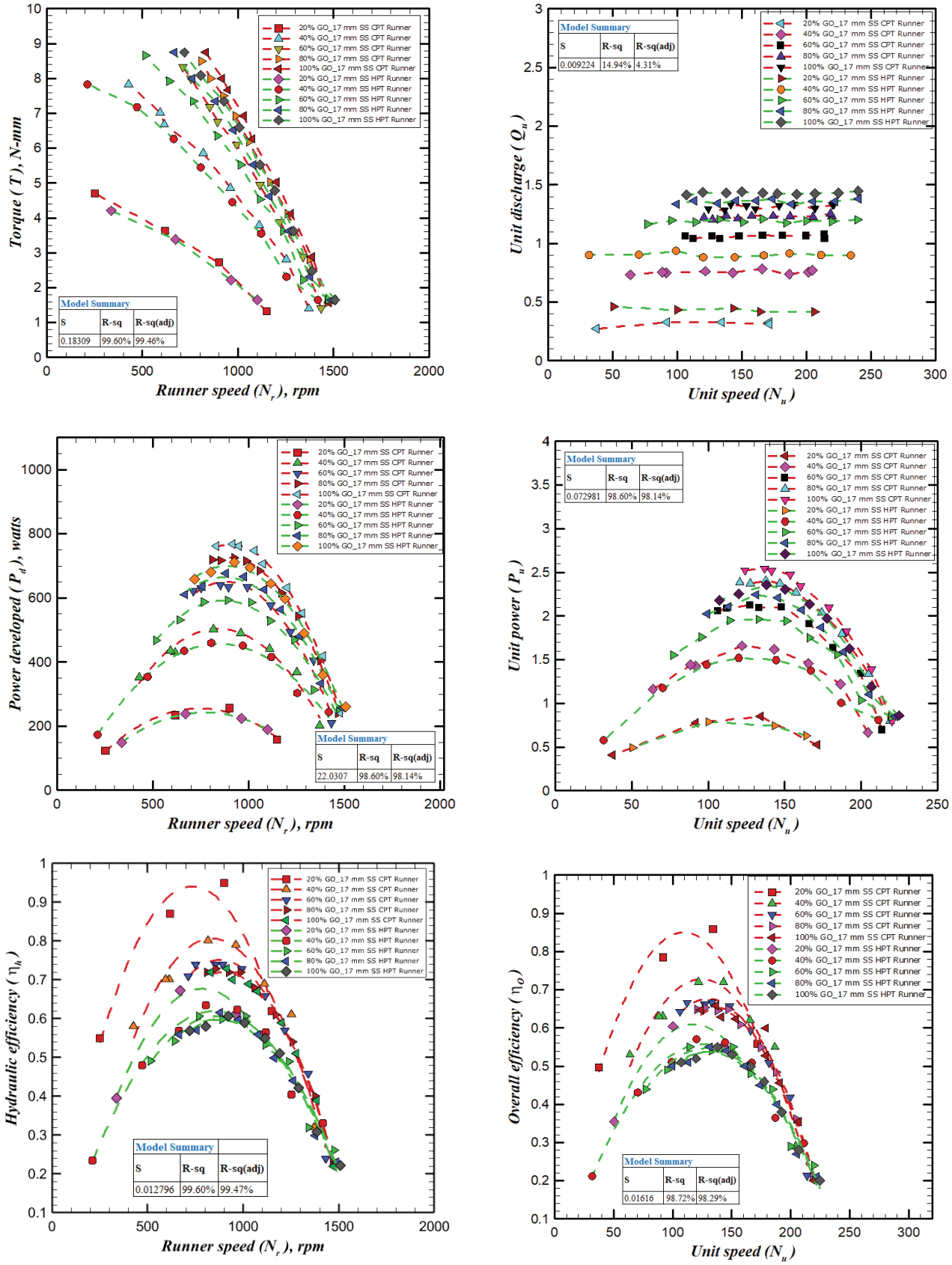

Figure 7. Main and operating characteristics with SSN1 17 mm nozzle.

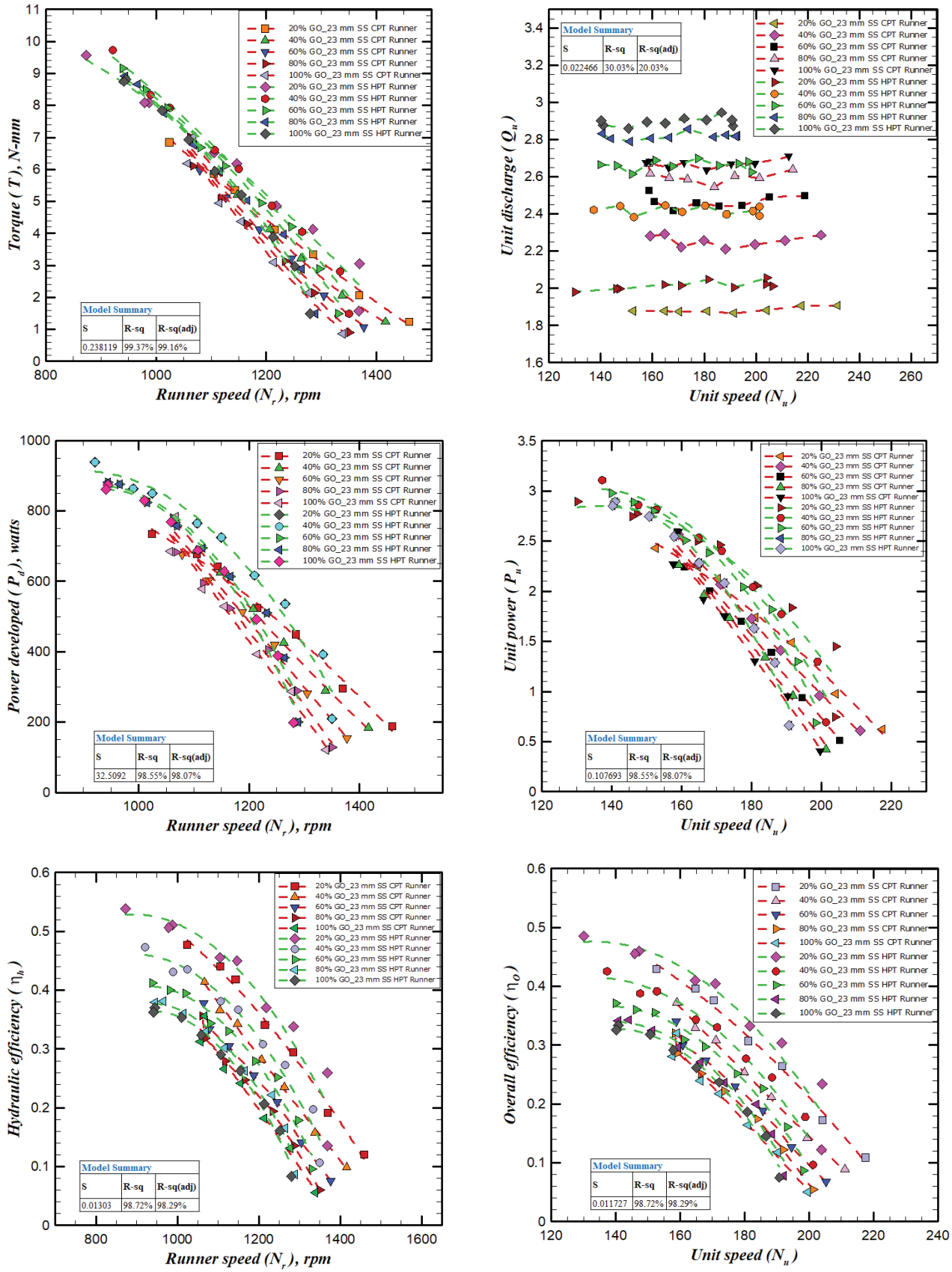

Figure 8. Main and operating characteristics with SSN2 23 mm nozzle.

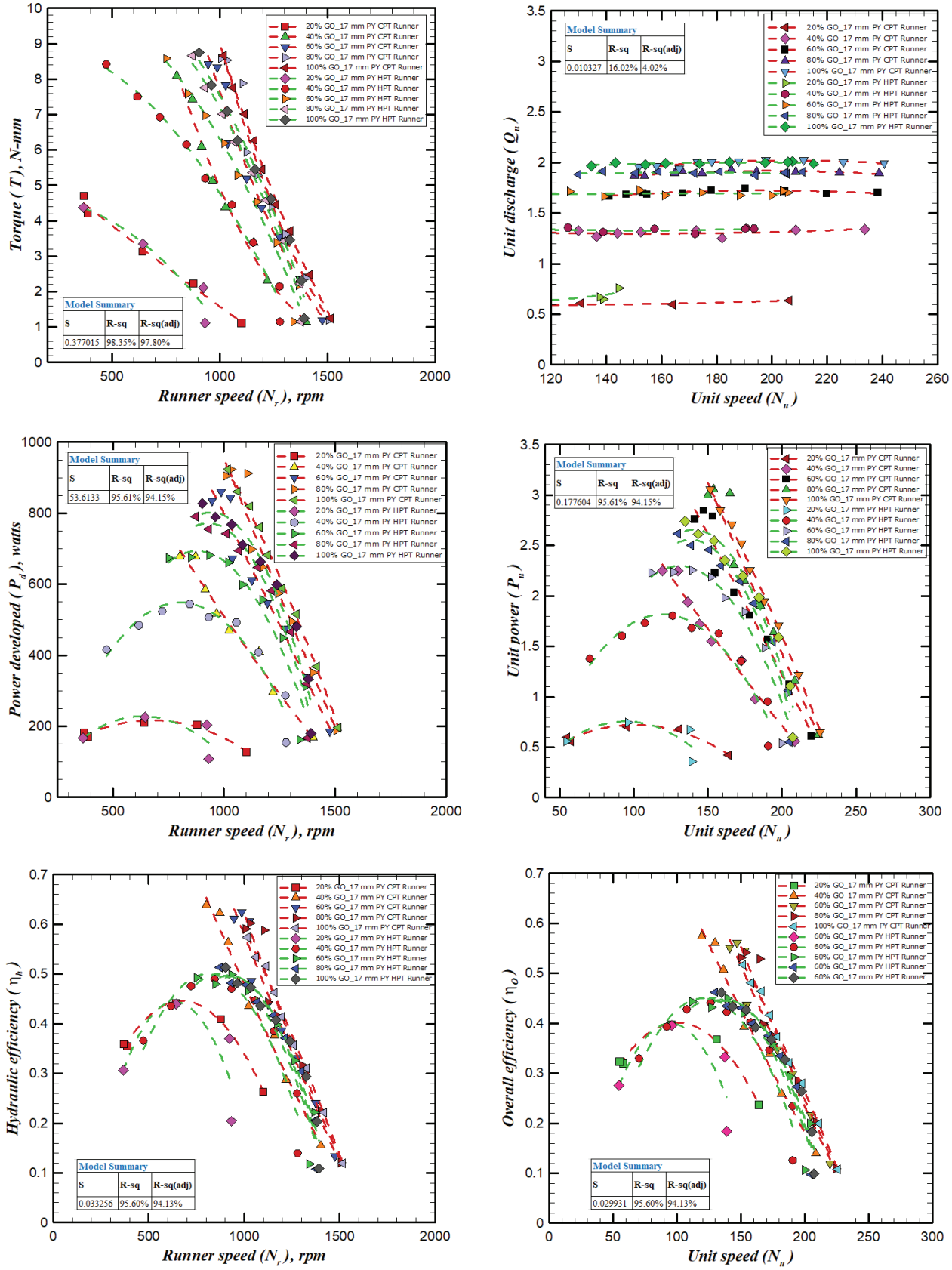

Figure 9. Main and operating characteristics with 17 mm Polymer nozzle (PYN1).

the nozzle's convergence angle is 24 degrees. The size of the jet was increased by 6 mm to check both runners' behavior under the increased water faucet. Figure 8 depicts the variation in flow rate, the corresponding change in parameters, and, ultimately, the efficiency. A broader spectrum in the right curve is covered with a 23 mm SSN2 nozzle, unlike a 17 mm diameter SSN1 nozzle. The flow area opened up to 40 %, giving maximum hydraulic efficiency for both runners due to fewer losses, but the curve spectrum is not fully covered as in the case with the ideal curve.

The points for parameters obtained with 23 mm SSN2 are separate and distinguishable. In Figure 8, the right-half curve is feasible only for the few restricted flow area percentages due to the heavy water faucet spilling out of the bucket without gliding and imparting work to the runner. The variation with the runner speed, a 17 mm diameter polymer nozzle (PYN1), exhibited a range of torque, power developed, and hydraulic efficiency.

Figure 9 shows the variation in unit speed plotted against unit discharge, unit power, and overall efficiency. The maximum hydraulic (η_h) and overall efficiencies (η_o) are noted with a 40 % gate opening with a conventional Pelton turbine (CPT) runner. The efficiencies corresponding to gate opening in each set can be represented as $\eta_h)_{CPT}$ is greater than $\eta_h)_{HPT}$ follows: The unit discharge (Q_u) remained equal for both runners. The hooped Pelton turbine runner (HPT) behaved equally for 40%, 60%, and 100% opening of the flow area for hydraulic efficiency.

The variation in main and operating characteristics is shown in Figure 10 with a polymer nozzle (PYN2) with an 18 mm exit diameter, 29-degree convergence angle(Θ_n), and 0.40 beta ratio(β). The speed range covered 400 -1500 rpm, and a smooth curve was obtained. The maximum hydraulic efficiency corresponds to 1011 rpm, which was found to be 53.11% in conventional Pelton turbine (CPT) runners, whereas it was found to be 52.34%, which corresponds to 963 rpm. The power developed at the runner shaft was measured with an absorption type dynamometer (rope brake type); in the case of a conventional Pelton turbine (CPT) runner, it is 890 watts, whereas, in the case of a hooped Pelton turbine (HPT) runner, it was 823.50 watt corresponding to 923 rpm of the runner.

Figure 11 depicts the variation in power developed, torque, and hydraulic efficiency with runner speed with a 19 mm diameter polymeric material nozzle (PYN3), a convergence angle of 30 degrees, and a beta ratio (β) of 0.42. The polymer material nozzle yielded the highest hydraulic efficiency, 61.66%, corresponding to 742 rpm of a hooped Pelton turbine (HPT) runner with only 20% of gate opening(GO). The unit quantities are also evaluated to check the runner's performance if the head changes.

Figure 12 shows the operating parameter for a 23 mm polymer nozzle (PYN4) with a beta ratio (β) of 0.29 and angle of convergence (Θ_n). In the present experimental study, the 23 mm polymer nozzle (PYN4) gave better efficiency at a lower rotation speed of runners in both Pelton turbine runner cases. The range of points and curves obtained with a 17 mm SS nozzle is similar to standard curves for the Pelton turbine. In the case of the CPT runner, the runner's speed of 1000 played a vital role as efficiency increases constantly.

Effect of the Nozzle Diameter for Various Nozzle Runner Combinations

The hydraulic efficiency of runners with 17 mm nozzles is higher than that of 23 mm because of the lower jet spreading and deviation. The 23 mm nozzles incurred more loss at the bucket and splashing in the visualization chamber. The mass of water trapped between the bucket and hoop plates in the hooped Pelton runner makes it heavy, apart from the weight of the hoop plates. There is more wake in the trapped system and water flow hindrance in the dynamic runner system instead of smooth gliding along the bucket's inner surface. For low speed, opt for a 17 mm stainless steel nozzle (SSN1), which $\eta_h)_{HPT}$ is greater than $\eta_h)_{CPT}$, as there are fewer losses in the confined space of bucket and hoop plates, which are dominant at high speed.

Figure 13 compares 17 mm and 23 mm diameter nozzles of stainless steel (SSN) and polymer (PYN) investigated for CPT and HPT runners under variable flow conditions. The torque for the 17 mm nozzle with the conventional Pelton turbine (CPT) runner must have a lower operating speed range than the hooped Pelton turbine (HPT) runner. The torque curve up to 1050 rpm due to momentum at low speed achieved through a 17 mm jet is dominant. The 17 mm and 23 mm polymer nozzles (PYN) have partiality in trends, but around 825 rpm with the conventional Pelton turbine (CPT) runner, the increase in torque occurs with a decrease in speed faster. In the present study, the hydraulic efficiencies with the same material but different jet diameters have been expressed as highest to lowest in $\eta_h)_{17mm,CPT}$, $\eta_h)_{17mm,HPT}$, $\eta_h)_{23mm,CPT}$, $\eta_h)_{23mm,HPT}$ order for polymer nozzles and $\eta_h)_{17mm,CPT}$, $\eta_h)_{23mm,HPT}$, $\eta_h)_{23mm,CPT}$, $\eta_h)_{17mm,HPT}$ for stainless steel nozzles up to a runner speed of 1100 rpm.

The nozzle diameter used here is 23 mm of stainless steel, and the beta ratio is kept for this nozzle. The size of the jet was increased by 6 mm to check both runners' behavior under the increased water faucet. The chart depicts the variation in flow rate and the corresponding change in parameters and, ultimately, the efficiency.

Effect of the Different Nozzle Materials for Various Nozzle Runner Combinations

The outward fluid flow occurs in a hooped Pelton turbine (HPT) runner bucket with two parts, as found during the experimental investigation. Also, it was found that the slots in a hoop plate with an opening govern the jet flow and outward stream through the bucket. The exhausting duration for the bucket full of water is significantly less due to high runner speed and confined space with a small slot in a hoop plate that retains most of the water in further

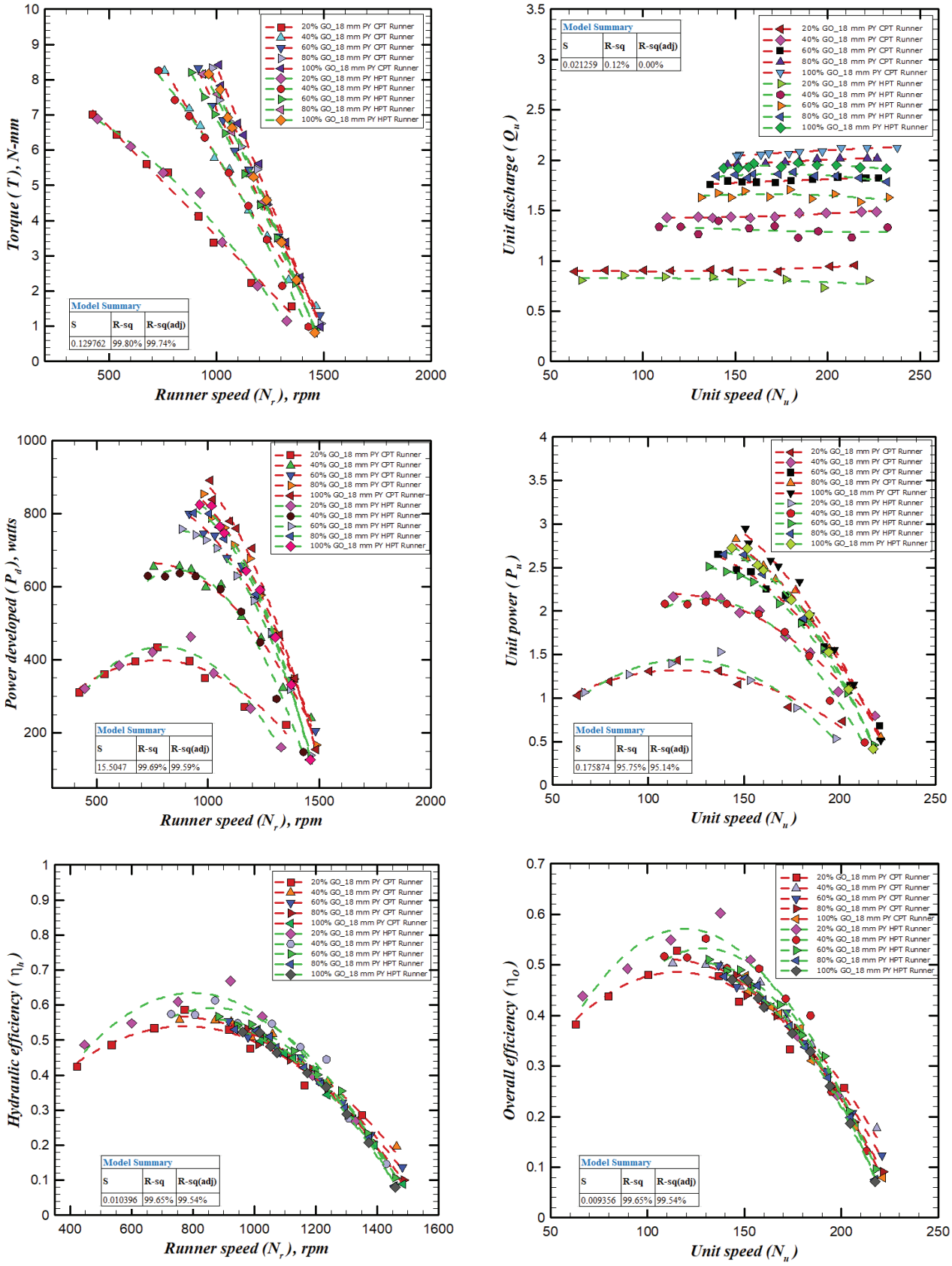

Figure 10. Main and operating characteristics with 18 mm polymer nozzle (PYN2).

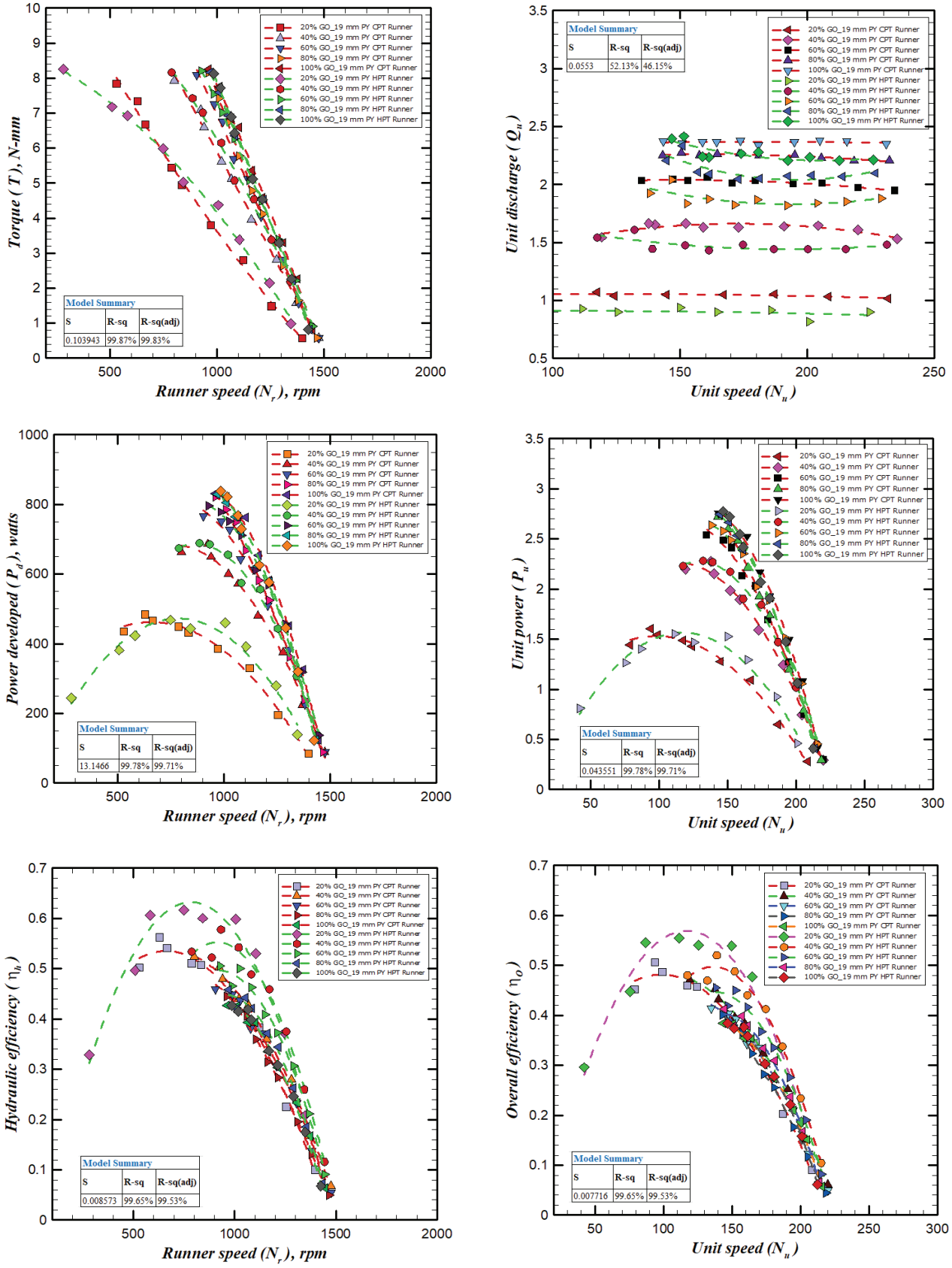

Figure 11. Main and operating characteristics with 19 mm polymer nozzle (PYN3).

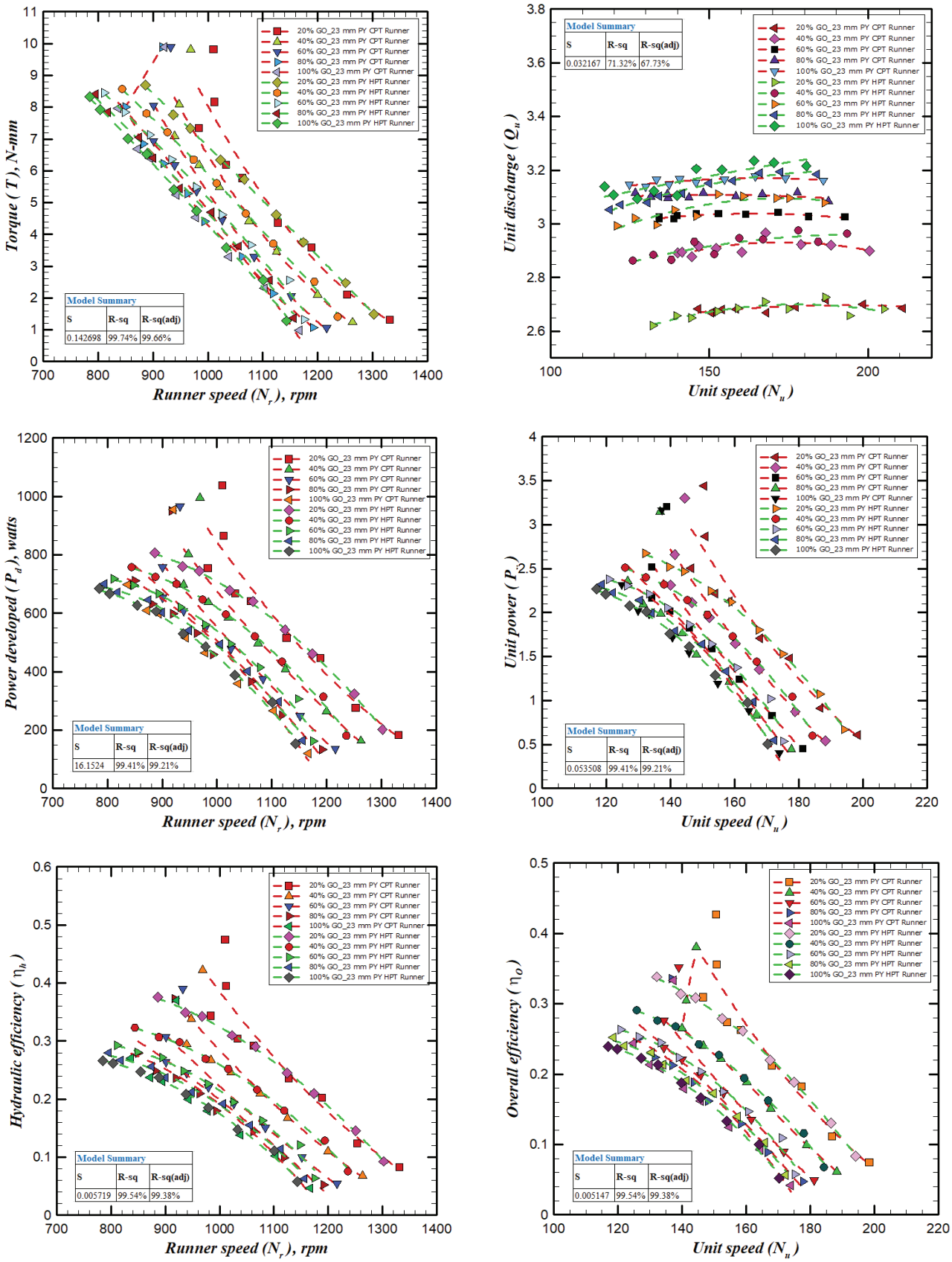

Figure 12. Main and operating characteristics with 23 mm polymer nozzle (PYN4)

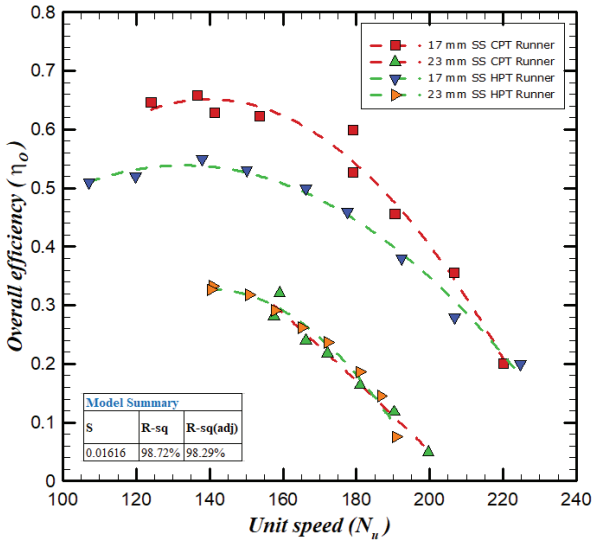
17 mm SS CPT Runner
23 mm SS CPT Runner
17 mm SS HPT Runner
23 mm SS HPT Runner
Overall efficiency (η_o)
Unit speed (N_u)
Model Summary
S R-sq R-sq(adj)
0.01616 98.72% 98.29%

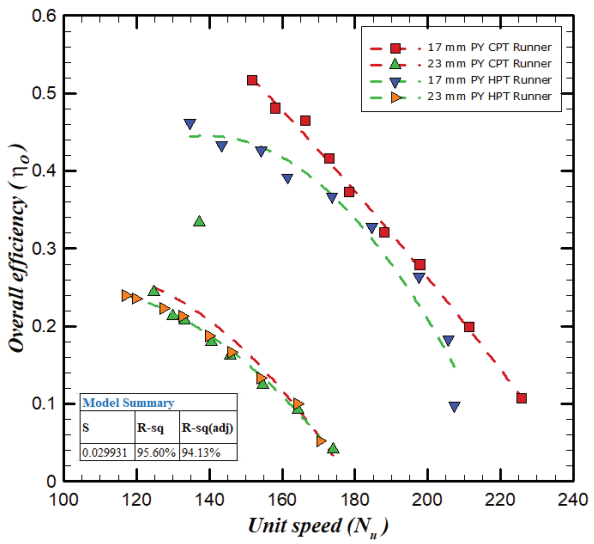
17 mm PY CPT Runner
23 mm PY CPT Runner
17 mm PY HPT Runner
23 mm PY HPT Runner
Overall efficiency (η_o)
Unit speed (N_u)
Model Summary
S R-sq R-sq(adj)
0.029931 95.60% 94.13%

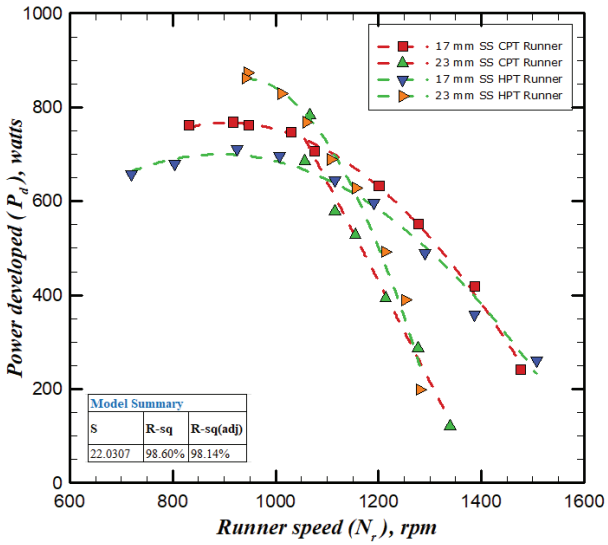
17 mm SS CPT Runner
23 mm SS CPT Runner
17 mm SS HPT Runner
23 mm SS HPT Runner
Power developed (P_d), watts
Runner speed (N_r), rpm
Model Summary
S R-sq R-sq(adj)
22.0307 98.60% 98.14%

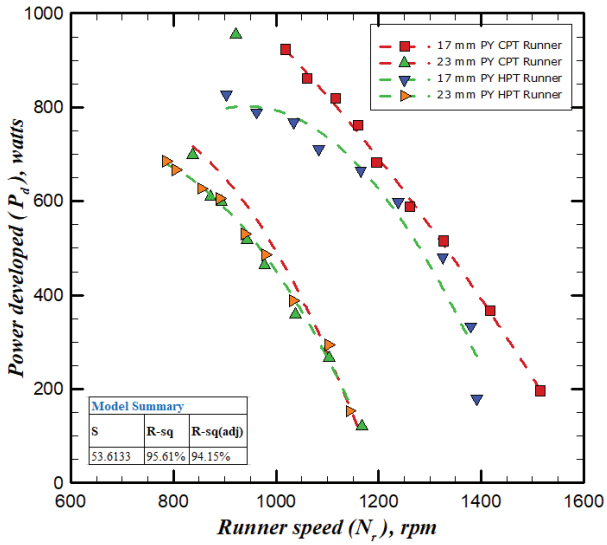
17 mm PY CPT Runner
23 mm PY CPT Runner
17 mm PY HPT Runner
23 mm PY HPT Runner
Power developed (P_d), watts
Runner speed (N_r), rpm
Model Summary
S R-sq R-sq(adj)
53.6133 95.61% 94.15%

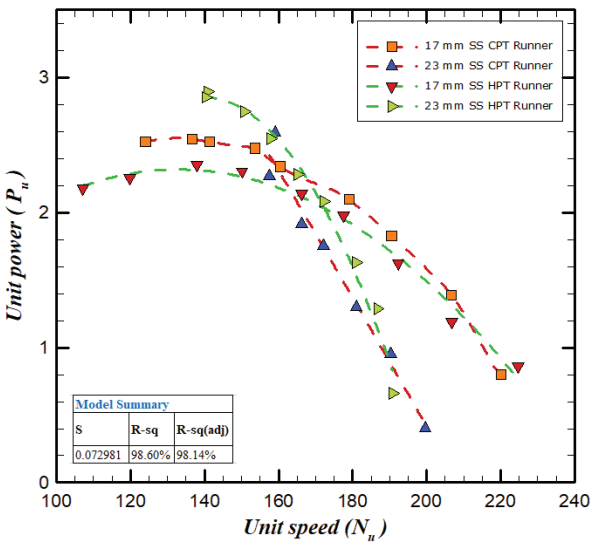
17 mm SS CPT Runner
23 mm SS CPT Runner
17 mm SS HPT Runner
23 mm SS HPT Runner
Unit power (P_u)
Unit speed (N_u)
Model Summary
S R-sq R-sq(adj)
0.072981 98.60% 98.14%

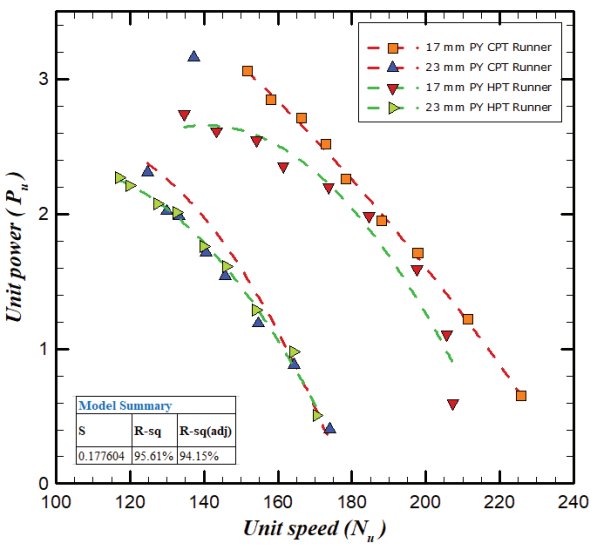
17 mm PY CPT Runner
23 mm PY CPT Runner
17 mm PY HPT Runner
23 mm PY HPT Runner
Unit power (P_u)
Unit speed (N_u)
Model Summary
S R-sq R-sq(adj)
0.177604 95.61% 94.15%

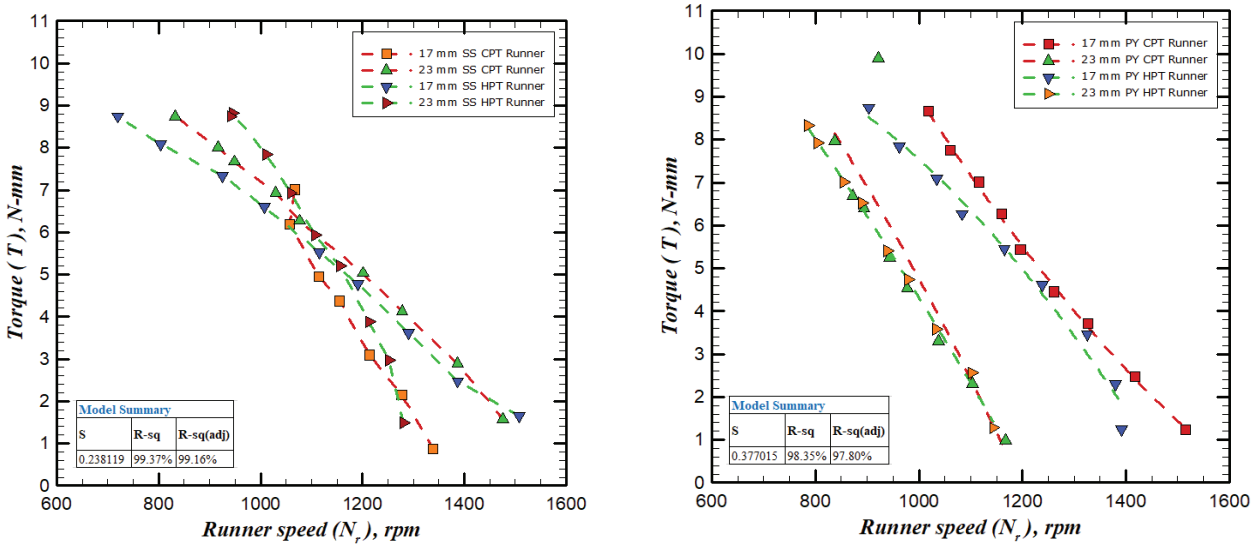

Figure 13. Main and operating characteristics for the different diameter nozzles for both runners.

rotation and falls due to gravity or centrifugal force without contributing much power to the runner shaft.

The variation in all the estimated parameters concerning runner speed is shown in Figure 14. The jet diffusion and separation of water particles from the jet surface at a larger jet diameter deteriorate the performance of the runners. The losses marked in the present study mainly include the higher diameter, the inertia of the turbine runner, and the obstructed outgoing flow with gradually increased gate opening (GO). The 17 mm diameter stainless steel nozzle (SSN1) has ticked all the boxes with fully defined performance characteristics, with variable area flow. The 23 mm nozzles suffer from jet stability and spread of jets despite less than 4Di distance. They further deteriorate the runner's performance with more water flow rates if used with a hooped Pelton turbine (HPT) runner compared to a conventional Pelton turbine (CPT) runner.

From the above graph, the hydraulic efficiencies (η_h) of all nozzle runner combinations in descending order can be written as $\eta_h)_{SSN1,CPT}$, $\eta_h)_{SSN1,HPT}$, $\eta_h)_{PYN1,CPT}$, $\eta_h)_{PYN2,CPT}$, $\eta_h)_{PYN2,HPT}$, $\eta_h)_{PYN1,HPT}$ for 17 mm (SSN1 and PYN1) and 18 mm (PYN2) nozzles. The $\eta_h)_{SSN1,CPT}$ combination has an 18.18% higher hydraulic performance compared to $\eta_h)_{PYN1,CPT}$ under the full gate open condition. The low-speed operation of small-diameter nozzles with heavier runner systems makes them more stable and valuable, as found in the case of an 18 mm polymer nozzle (PYN2), and can be a substitute for 17 mm nozzles with a higher convergence angle(Θ_n). The 19 mm polymer nozzles with a 30-degree convergence angle(Θ_n) and beta ratio(β) of 0.42 have almost the same performance for 100% gate opening, which $\eta_h)_{PYN3,CPT}$ is equal to $\eta_h)_{PYN3,HPT}$. A 19 mm Polymer nozzle (PYN3) achieves the optimum nozzle diameter here, similar to a 23 mm Polymer nozzle (PYN4), where hydraulic efficiency points coincide and are non-distinguishable, which $\eta_h)_{PYN4,CPT}$ is equal to $\eta_h)_{PYN4,HPT}$. The larger diameter stainless steel nozzle (SSN2) of 23 mm was tested with both runners, but the hydraulic efficiency (η_h) of the runners was found with the whole gate opening (100%) in the order of $\eta_h)_{SSN2,CPT}$ is greater than $\eta_h)_{SSN2,HPT}$. However, jet size, even for a conventional Pelton runner (CPT), plays a vital role in the hydraulic performance of the runner. Even with the larger flow area and, hence, higher fluid flow rate, the efficiency of a conventional Pelton runner (CPT) yielded 35.63% at 1067 rpm of the runner, whereas it was found to be 75.14% at 914 rpm of the runner with less flow area and a whole gate opening.

The work carried out by various authors has been mentioned in Table 5. The essential parameters like head, PCD of the turbine runner, nozzle diameter, and Number of nozzles employed for the experimental investigation, are mentioned. The experimental work on HPT is limited to numerical simulation and single-diameter nozzle efficiency evaluation. The regime beyond the single diameter was explored here to reveal the hydraulic characteristics of HPT.

Figure 15 shows the variation in hydraulic efficiency for comparison in the vertical bar chart. The comparison shows the variation in the efficiency range for the parameters considered in the present study. The chart was plotted with a 17 mm nozzle with a full gate opening. The available data are compared since the experimental work is limited to the HPT runner.

Figure 16 compares and supports the trend obtained from the present experimental observations. The trend line has suggested that the efficiency of the present work is behaving similarly to the previous work of different authors. The characteristics of CPT and HPT are the same but offset by some distance depending upon the additional inertia offered by adding hoop plates. In the present study, the graph shows that the hydraulic efficiency trend line is apart by 15.09% at low runner speed, though it started at high rpm.

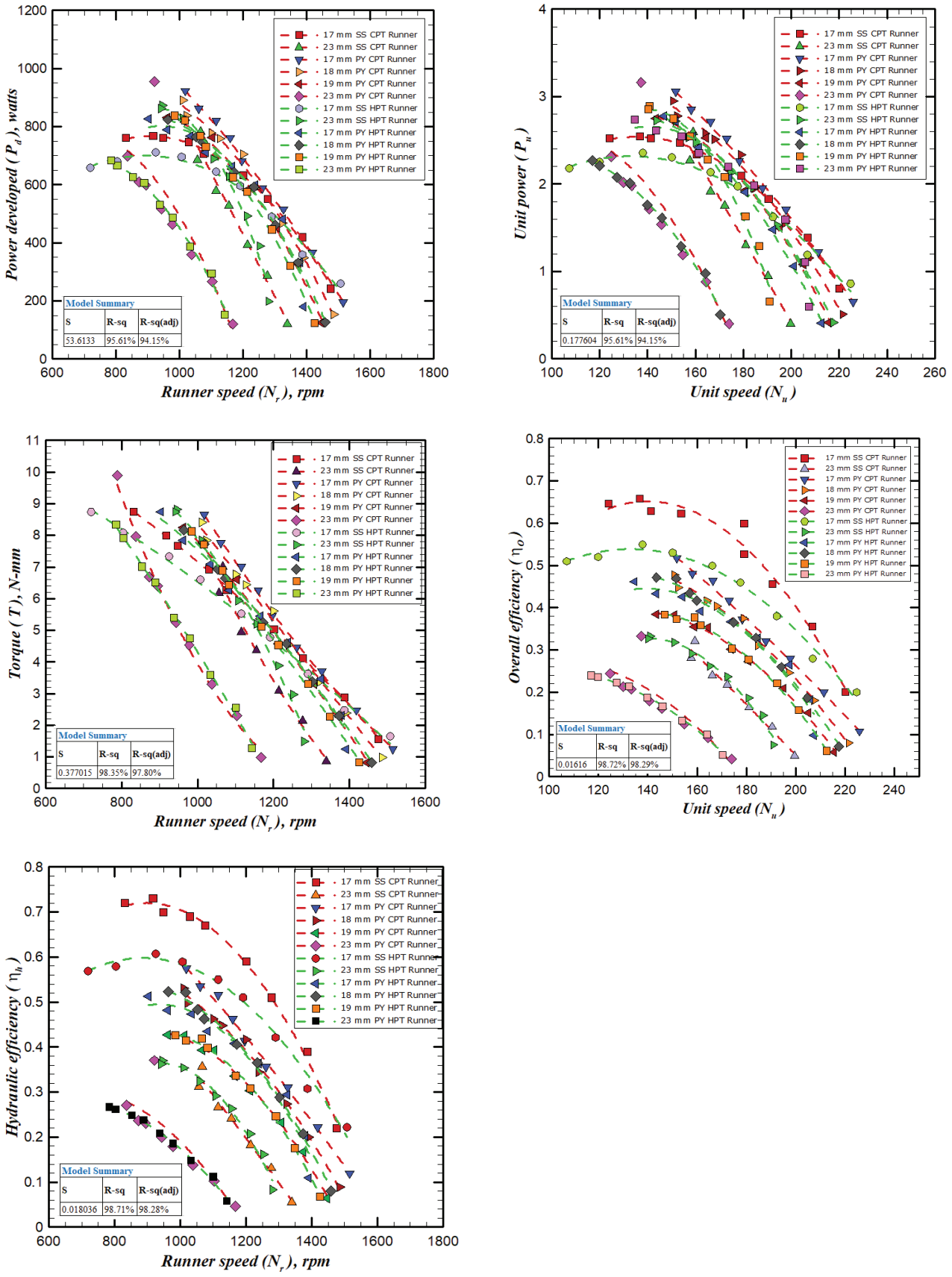

Figure 14. Main and operating characteristics for all the nozzle-runner combinations.

Table 5. Summary for comparison of present and similar past work

Sr. No.	Author/s	Parameters considered	Type of work carried out	Hydraulic efficiency (η_h)
1	Rafae Alomar et al., 2022 [70]	CPT, Head = 113 m, Runner diameter =275 mm, nozzle diameter = 9.5-12.5 mm (4 nos. in equal steps), Number of nozzles=1	Experimental	35.5-21.6%
2	Syofii et al., 2022 [71]	CPT, Head = 3 m, Runner diameter = 275 mm, nozzle diameter= 8 ,9, 10 mm, Number of nozzles=1	Experimental	9.01-25.44%
3	Elgammi & Hamad, 2022 [72]	CPT, Head = 2.5 m, Runner pitch circle diameter =123 mm, nozzle diameter= 9 mm, Number of nozzles=8	Experimental	10%
4	Hlabanelo et al., 2020 [73]	CPT,Head = 10 m, Runner diameter =220 mm, nozzle diameter = 21 mm, Number of nozzles=2	Experimental and numerical	5-64%
5	Nigussie et al., 2017 [74]	CPT,Head = 47.5 m, Runner pitch circle diameter = 500 mm, nozzle diameter= 38.50 mm, Number of nozzles=4	Numerical	78.8%
6	Cobb & Sharp, 2013	CPT, Runner pitch circle diameter =100 mm, head =17-25 m and 18- 28 m, nozzle diameter = 7.94 to 12.70 mm, Number of nozzles =1	Experimental	73%
7	Chaudhari et al.,2011	CPT,HPT Head = 45 m, Runner pitch circle diameter = 360 mm, nozzle diameter = max 260 mm, Number of nozzles=1	Experimental and numerical	52%,45%
8	Present study	CPT,HPT Head = 43 m, Runner pitch circle diameter = 256 mm, nozzle diameter = 17,18,19 and 23 mm, Number of nozzles=1	Experimental	For CPT and HPT

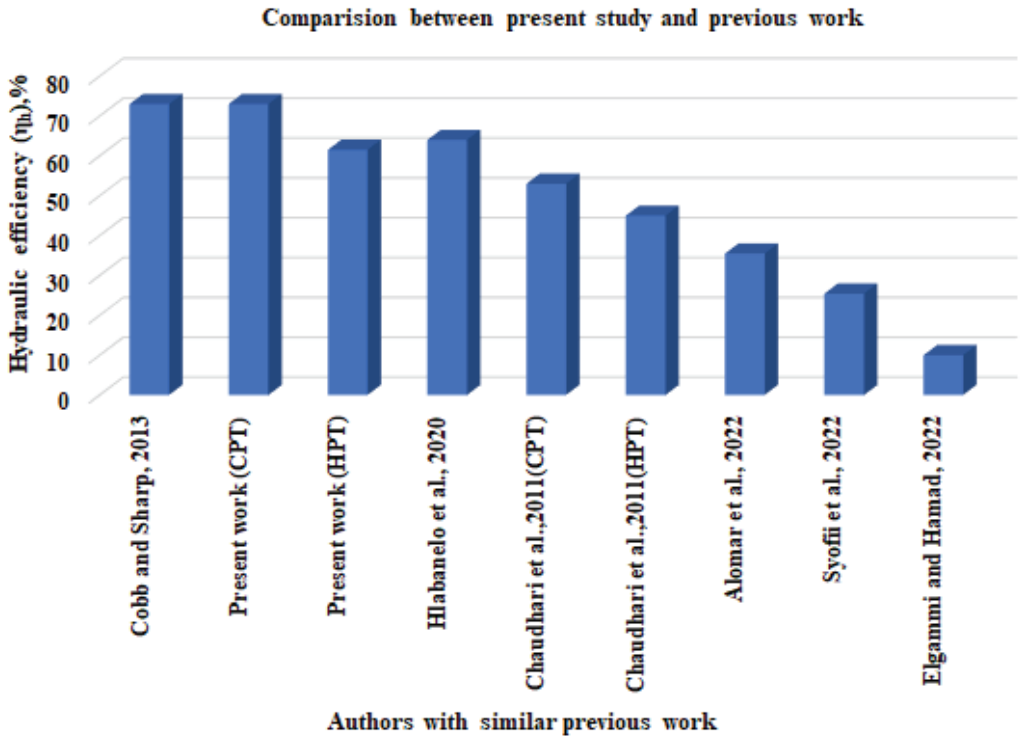

Figure 15. A hydraulic efficiency comparison bar chart of the present work with previous similar work.

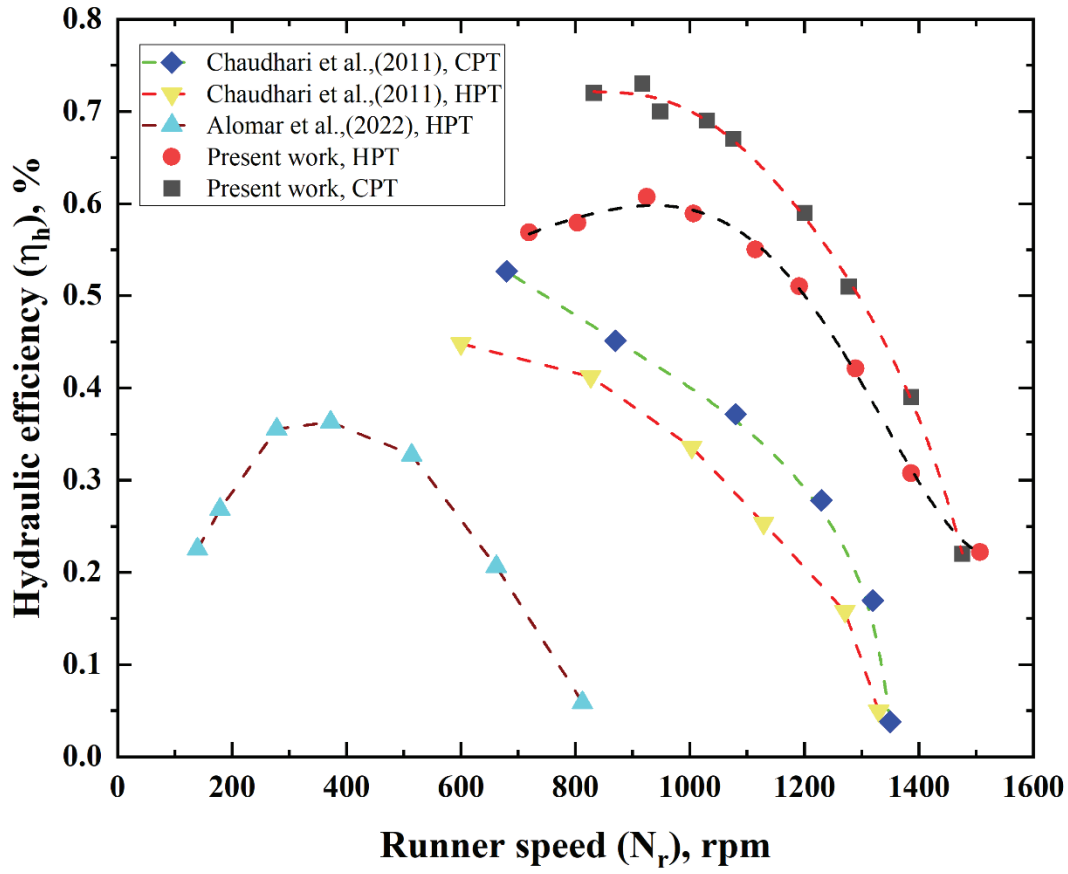

Figure 16. Hydraulic efficiency(η_h) vs Runner speed (N_r) - comparison for runners of the present work with previous similar work.

UNCERTAINTY ANALYSIS

According to the study, the uncertainty found for the head of water, angular speed, torque developed at the runner shaft, and flow rate is given in Appendix 1 with the whole gate opening (100%) for all the tested combinations. Equation (8) defines the hydraulic efficiency of the turbine runner, and the corresponding Equation (9) for uncertainty is used to calculate values.

$$\eta_h = \frac{T\omega}{\rho g Q H} \tag{8}$$

Since the experiments were carried out with a constant head, but considering frictional head loss and pipe fitting loss incurred to calculate the value of dH, the difference in measured and actual value of torque due to spring balance, which is taken care of by considering the most minor count. The measured value from the speed sensor and flow rate is also affected by the accuracy and subsequent error in measurement.

$$\frac{d\eta_h}{\eta_h} = \sqrt{\left(\frac{dH}{H}\right)^2 + \left(\frac{dT}{T}\right)^2 + \left(\frac{d\omega}{\omega}\right)^2 + \left(\frac{dQ}{Q}\right)^2} \tag{9}$$

According to the study, a sample calculation for uncertainty with a whole gate opening (100%) corresponding to maximum hydraulic efficiency is calculated as per Equation (9) and given in Appendix 1. The arrangement in the case of a conventional Pelton turbine (CPT) runner found for the available head, torque, angular speed, and flow rate was ±0.48%, ±1.33%, ±1.19%, and ±0.01%, respectively, and uncertainty in hydraulic efficiency corresponding to that found to be ±1.31% with arrangement of the Hooped Pelton Turbine (HPT) runner and 23 mm Polymer nozzle (PYN) combination.

CONCLUSION

In addition to the flow rate(Q), jet size (Di), Speed ratio(ϕ), and jet ratio(m), the runner's performance is also affected by both centrifugal and Coriolis forces. The literature review shows that varying operating conditions like

nozzle diameter (Di) and water discharge (Q) significantly impact Pelton turbine performance.

In the current study, the SSN1, SSN2, PYN1, PYN2, PYN3, and PYN4 nozzles were used to estimate the performance of the runners. The different diameters of the nozzle are the same in construction and materials, except for the beta ratio(β) and angle of convergence (Θ_n). The runners were tested for varying flow conditions to get hydraulic performance and subsequent comparison. The jet ratio (m) and the nozzle convergence angle (Θ_n) were in the range of 11 to 15 and 24 to 32 degrees, respectively.

The following are the conclusions drawn from the present experimental investigations,

- The nozzle with a more than 17 mm diameter (D_i) has reduced potential energy available at exit as the discharge increases. The subsequent velocity also reduces. The water input power (P_{in}) to the turbine reduces with an increase in the nozzle diameter. Thus, the increase in nozzle diameter reduces the turbine's hydraulic efficiency(η_h).
- The higher beta ratio yielded low hydraulic efficiency as the losses dominated in the larger-diameter jet. The effect of convergence angle (Θ_n) is also practical, as it inversely suggests hydraulic efficiency. The 17 mm nozzles with the highest convergence angle (Θ_n) of 32 degrees have contributed more to the hydraulic performance of either runner.CPT tested with a higher convergence angle (Θ_n) nozzle has yielded 18.18% more efficiency than HPT.
- The nozzles with a jet ratio(m) of 15 were more suitable for the runners. The main and operating characteristics curves have been entirely over the range of runner speeds. The decreasing jet ratio has reduced jet stability, affecting the turbine's hydraulic performance.
- The runners were tested with a range of velocity ratios (ϕ = u/Vjet) of 0.423 to 0.492. The CPT was most efficient with a velocity ratio (ϕ) of 0.423. The HPT with a higher nozzle diameter and a nozzle opening between 20% and 40 % has the least inertia due to the flow through the bucket without diffusion in the void between hoop plates.
- In the case of runners, the CPT has higher hydraulic efficiency(η_h), approximately 20% higher than the hooped Pelton turbine runner at the pick point for all nozzle runner combinations. Still, that offset margin in the curve gradually decreases with increased speed. The speed and nozzle diameter combination best suits a 17 mm stainless steel nozzle (SSN1), 900 rpm, with a conventional Pelton turbine (CPT) runner, 100% gate opening.
- It was found that the same material, the hooped Pelton turbine (HPT) runner and 23 mm stainless steel nozzle (SSN2), produce the highest torque but have less hydraulic efficiency due to losses in the void created between bucket and hoop plates. However, it cannot be discarded for other reasons, such as suggesting benefits like bucket strength under heavy jet from the faucet.
- The larger diameter in the polymeric nozzle (PYN) gave low performance compared to the smaller diameter nozzle, i.e., 17 mm. In the case of both runners, a 17 mm diameter nozzle was found most appropriate for a given runner's dimensions. This could be because of the reduced jet diffusion provided by the hoop with a smaller diameter nozzle, which handles the outgoing proportion of fluid in equal amounts through the slots on the hoop plates.
- The efficiency difference between both runners is more pronounced at higher gate openings due to the significant flow passage being impeded by the hoop plates. At lower gate openings, the hoop plates obstruct the smaller flow route less, making the efficiency difference less noticeable.
- The hoop plates support the buckets, which are cantilever parts bolted to the dynamic runner system. During experimentation, the bifurcated jet and outgoing water splashing on the runner's hoop are visible in the flow contours. This water splashing, more pronounced with larger gate openings, is the primary cause of efficiency decline. The speed and flow area at the spear-nozzle assembly are crucial for hydraulic efficiency.

This experimental investigation has provided vital details regarding the effect of varying flow area, jet ratio, speed ratio, and convergence angle on the performance of a Hooped Pelton Turbine (HPT) runner compared to an identically sized Conventional Pelton Turbine (CPT) runner. This study also forms the basis for optimizing the hoop gap and slot opening size over the hemispherical bucket to provide the least impedance to the outgoing fluid stream.

NOMENCLATURE

Q	Volumetric flow rate/Discharge m^3/hr
D_o	Inlet diameter of the nozzle or inside diameter of the pipe, mm
D_i	Exit diameter of the nozzle, mm
D	Diameter of the brake drum, m
D_r	Diameter of rope, m
D_e	Effective diameter of the drum, m
D_P	Pitch Circle Diameter of the runner, mm
R_e	Reynolds number
H	Available head, m
Q_u	Unit discharge
N_u	Unit speed
N_r	Runner speed, rpm
P_u	Unit power
P_d	Power developed, Watt
P_{in}	Power input, kW
V_{jet}	The velocity of the fluid, m/s
u	Peripheral velocity of runners, m/s
T_d	Torque developed, N-m
m	Jet ratio
g	Gravitational constant, m/s^2

Greek Symbols

ρ	The density of the fluid, kg/m^3
β	Beta ratio- a ratio of the nozzle outlet to the inlet
β_2	The jet angle at the bucket exit, degrees
ω	Angular speed of the runner, rad/sec
η_o	Overall efficiency
η_h	Hydraulic efficiency
ϕ	Speed ratio/ Velocity ratio
Θ_n	Angle of convergence for the nozzles, degrees

Abbreviations

SSN	Stainless Steel Nozzle
PYN	Polymer Nozzle (Polyacetal or Polyoxymethylene)
CPT	Conventional Pelton Turbine
HPT	Hooped Pelton Turbine
GO	Gate Opening

Subscript

2	Refers to exit
d	Refers to the developed
e	Refers to effective
h	Refers to hydraulic
n	Refers to the nozzle
o	Refers to overall
u	Refers to the unit

Future Scope of Work

The work can be extended for numerical simulation to model the effect of the hoop gap on the performance of runners. The analytical and subsequent numerical simulation for the flow area gap in the hoop plate can be modeled. The hoop plate can be made of lightweight material like aluminum to reduce the inertia and increase hydraulic performance.

ACKNOWLEDGMENT

Thanks to *Dr. S. A. Channiwala* and *Dr. G. C. Chaudhari* for supporting the experimentation and also permitting the test facility at Advance Fluid Mechanics and Fluid Power (AFM & FP) Laboratory, Sardar Vallabhbhai National Institute of Technology (SVNIT), Surat, Gujarat, India. The test facility is the same one used by the author for work carried out in studying jet expansion.

AUTHORSHIP CONTRIBUTIONS

Dr. V. K. Patel: Reviewed the manuscript and gave expert advice as a supervisor. **Prof. H. N. Lakdawala, Trupal R. Patel:** Experimentation, data collection, and prepared manuscript. **N Bagre:** Graph plotting and image processing. **Dr. S. A. Channiwala** and **Dr. G. C. Chaudhari:** Conceived the idea and developed the test facility.

DATA AVAILABILITY STATEMENT

The authors confirm that the article's data supporting this study's findings are available. Raw data supporting this study's findings are available from the corresponding author upon reasonable request.

CONFLICT OF INTEREST

The author declared no potential conflicts of interest concerning this article's research, authorship, and/or publication.

ETHICS

There are no ethical issues with the publication of this manuscript.

STATEMENT ON THE USE OF ARTIFICIAL INTELLIGENCE

Artificial intelligence was not used in the preparation of the article.

REFERENCES

[1] Alnakhlani MM, Mukhtar, Himawanto DA, Alkurtehi A, Danardono D. Effect of the bucket and nozzle dimension on the performance of a Pelton water turbine. Mod Appl Sci 2015;9:25-33. [CrossRef]

[2] Zeng C, Xiao Y, Yongyao, L, Jin Z, Zhengwei W, Honggang F, et al. Hydraulic performance prediction of a prototype four-nozzle Pelton turbine by entire flow path simulation. Renew Energy 2018;125:270–282. [CrossRef]

[3] Alam MMA, Setoguchi T, Matsuo S, Kim HD. Nozzle geometry variations on the discharge coefficient. Propuls Power Res 2016;5:22–33. [CrossRef]

[4] Zhang Z, Casey M. Experimental studies of the jet of a Pelton turbine. Proc Inst Mech Eng A J Power Energy 2007;221:1181–1192. [CrossRef]

[5] Donaldson CD, Snedeker RS. A study of free jet impingement. Part 1. Mean properties of free and impinging jets. J Fluid Mech 1971;45:281–319. [CrossRef]

[6] Santolin A, Cavazzini G, Ardizzon G, Pavesi G. Numerical investigation of the interaction between jet and bucket in a Pelton turbine. Proc Inst Mech Eng A J Power Energy 2009;223:721–728. [CrossRef]

[7] Xiao Y, Liu Z, Liang Q, Liu J, Zhang J, Zhu Y, et al. The interaction between bucket number and performance of a Pelton turbine. Energy 2024;287:129646. [CrossRef]

[8] Gupta V, Prasad V. Numerical investigations for jet flow characteristics on Pelton turbine bucket. Int J Emerg Technol Adv Eng 2012;2:364–370.

[9] Gupta V, Prasad V, Khare R. Effect of jet length on the performance of Pelton. 2016;11:11487–11494.

[10] Obayes SA, Qasim MA. Effect of flow parameters on Pelton turbine performance by using different nozzles. Int J Model Optim 2017;7:128–133. [CrossRef]

[11] Nyantekyi-Kwakye B. Experimental examination of nozzle geometry on water jet in a subsonic crossflow (Master thesis). Canada: University of Manitoba; 2011.
[12] McCarthy MJ, Molloy NA. Review of stability of liquid jets and the influence of nozzle design. Chem Eng J 1974;7:1-20. [CrossRef]
[13] Jo IC, Park JH, Kim JW, Shin Y, Chung JT. Jet quality characteristics according to nozzle shape of energy-recovery Pelton turbines in pressure-retarded osmosis. Desalination Water Treat 2016;57:24626–24635. [CrossRef]
[14] Gass BM, Hetchy Water H. Modification of nozzles for the improvement of efficiency of Pelton type turbines. 2002. Available at: https://api.semanticscholar.org/CorpusID:56348066 Accessed on Jan 28, 2026.
[15] Unterberger P, Unterberger P, Bauer C, Gaschl J, Mack R. Studies on the free jet of Pelton nozzles. 2010. Available at: https://www.researchgate.net/publication/260508415_Studies_on_the_free_jet_of_pelton_nozzles Accessed on Jan 28, 2026.
[16] Tesař V. Characterisation of inexpensive, simply shaped nozzles. Chem Eng Res Des 2010;88:1433–1444. [CrossRef]
[17] Vahedi Tafreshi H, Pourdeyhimi B. The effects of nozzle geometry on waterjet breakup at high Reynolds numbers. Exp Fluids 2003;35:364–371. [CrossRef]
[18] Kartashev AL, Kartasheva MA. Designing of optimal annular nozzles with multiphase flows. Procedia Eng 2016:161–167. [CrossRef]
[19] Adhikari RC, Wood DH. A new nozzle design methodology for high efficiency crossflow hydro turbines. Energy Sustain Dev 2017;41:139–148. [CrossRef]
[20] Staubli T, Abgottspon A, Weibel P, Bissel C. Jet quality and Pelton efficiency: Effects of suspended sediment on Pelton turbine wear and efficiency. Conference Paper. In: Hydro 2009 At: Lyon, France 2009.
[21] Na S. Simulation of unsteady water film flow on Pelton bucket. Energy Power Eng 2013;5:51–55. [CrossRef]
[22] Perrig A, Avellan F, Kueny JL, Farhat M, Parkinson E. Flow in a Pelton turbine bucket: Numerical and experimental investigations. J Fluids Eng 2006;128:350–358. [CrossRef]
[23] Zeng C, Xiao Y, Wang Z, Zhang J, Luo Y. Numerical analysis of a Pelton bucket free surface sheet flow and dynamic performance affected by operating head. Proc Inst Mech Eng A J Power Energy 2017;231:182–196. [CrossRef]
[24] Papantonis DE, Anagnostopoulos JS, Papantonis DE. A numerical methodology for design optimization of Pelton turbine runners: Design optimisation of Pelton and Turgo type water turbine's injectors. 2006. Available at: https://www.semanticscholar.org/paper/A-numerical-methodology-for-design-optimization-of-Anagnostopoulos-Papantonis/35d7fd57c36b75fc4ddd5734f94f7ab70906f6d0 Accessed on Jan 28, 2026.
[25] Solemslie BW, Dahlhaug OG. A reference Pelton turbine design. IOP Conf Ser Earth Environ Sci 2012;22:012004. [CrossRef]
[26] Kumashiro T, Fukuhara H, Tani K. Unsteady CFD simulation for bucket design optimization of Pelton turbine runner. IOP Conf Ser Earth Environ Sci 2016;49:022003. [CrossRef]
[27] Chapuis L, Froschl K. Optimized fabrication of Pelton turbine runners. Int J Hydropower Dams 1998;5:30–32.
[28] Neopane HP, Thapa B, Panthee A, Neopane HP. CFD analysis of Pelton runner. Int J Sci Res Publ 2014;4:1-6.
[29] Chaudhari GC, Shah SP, Channiwala SA. A hooped Pelton runner: FE analysis and experimentation. In: Proceedings of ASME Turbo Expo 2011 GT2011 June 6-10, 2011, Vancouver, British Columbia, Canada. [CrossRef]
[30] Sabu S, Antony TA, George NJ, Chandy A, Asst A, Jyothi A. Design and modelling of a Pelton wheel bucket: Theoretical validation and software comparison. Int J Eng ResTechnol 2014;3:2271-2273.
[31] Chaudhari G, Shah S, Channiwala S, Kulshreshtha D. Flow visualization study of jet and bucket interactions in traditional and hooped Pelton runner. In: ASME-JSME-KSME 2019 8th Joint Fluids Engineering Conference, 2019. [CrossRef]
[32] Chaudhari GC, Channiwala SA, Shah SP. Comparative assessment of the developed stress in both traditional and hooped Pelton runners. Proceedings of ICFD 10: Tenth International Congress of Fluid Dynamics December 16-19, 2010, Stella Di Mare Sea Club Hotel, Ain Soukhna, Red Sea, Egypt.
[33] Li JQ, Myat M, Saw M. Fatigue analysis of simple and advanced hoop Pelton turbine buckets. Am Sci Res J Eng 2017;29:371–378.
[34] Karna A, Chitrakar S, Bhurtel M, Baral B, Solemslie BW. Numerical analysis of traditional and hooped Pelton runner at various operating conditions. J Phys Conf Ser 2023;231:182-196. [CrossRef]
[35] Chaudhari G, Channiwala S, Shah S, Kulshreshtha D. Experimental investigation on effect of hoop thickness on performance of hooped Pelton wheel. J Phys Conf Ser 2023;2629:012003. [CrossRef]
[36] Gupta V, Khare R, Prasad V. Performance evaluation of Pelton turbine: A review. Hydro Nepal J Water Energy Environ 2014;13:28–35. [CrossRef]
[37] Sani AE. Design and synchronizing of Pelton turbine with centrifugal pump in RO package. Energy 2019;172:787–793. [CrossRef]

[38] Osterwalder J. Efficiency scale-up for hydraulic turbo-machines with due consideration of surface roughness. J Hydraul Res 1978;16:55–76. [CrossRef]
[39] Rossetti A, Santolin A, Cavazzini G, Pavesi G, Ardizzon G. Analysis of Pelton bucket efficiency. In: The 9th European Conference on Turbomachinery Fluid Dynamics and Thermodynamics. 2011. [CrossRef]
[40] Rossetti A, Pavesi G, Cavazzini G, Santolin A, Ardizzon G. Influence of the bucket geometry on the Pelton performance. Proc Inst Mech Eng A J Power Energy 2014;228:33-45. [CrossRef]
[41] Jošt D, Mežnar P, Lipej A. Numerical prediction of Pelton turbine efficiency. IOP Conf Ser Earth Environ Sci 2010;12:012080. [CrossRef]
[42] Zeng CJ, Xiao YX, Zhang J, Gui ZH, Wang SH, Luo YY, et al. Numerical prediction of hydraulic performance in model and homologous prototype Pelton turbine. IOP Conf Ser Earth Environ Sci 2018;163:012016. [CrossRef]
[43] Han L, Zhang GF, Wang Y, Wei XZ. Investigation of erosion influence in distribution system and nozzle structure of Pelton turbine. Renew Energy 2021;178:1119–1128. [CrossRef]
[44] Stamatelos FG, Anagnostopoulos JS, Papantonis DE. Performance measurements on a Pelton turbine model. Proc Inst Mech Eng A J Power Energy 2011:351–362. [CrossRef]
[45] Cobb BR, Sharp KV. Impulse (Turgo and Pelton) turbine performance characteristics and their impact on pico-hydro installations. Renew Energy 2013;50:959–964. [CrossRef]
[46] Chávez JC, Valencia JA, Jaramillo GA, Coronado JJ, Rodríguez SA. Failure analysis of a Pelton impeller. Eng Fail Anal 2015;48:297–307. [CrossRef]
[47] Patel K, Patel B, Yadav M, Foggia T. Development of Pelton turbine using numerical simulation. IOP Conf Ser Earth Environ Sci 2010;12:012048. [CrossRef]
[48] Muhibbuddin, et al. Analysis of the performance for runner Pelton turbine by using bamboo material. J Adv Res Fluid Mech Therm Sci 2021;79. [CrossRef]
[49] Woodcock DJ, White IM. The application of Pelton type impulse turbines for energy recovery on seawater reverse osmosis systems. Desalination 1981;39:1-3. [CrossRef]
[50] Güven AF. A comparative study on hybrid GA-PSO performance for stand-alone hybrid energy systems optimization. Sigma J Eng Nat Sci 2024;42:1410–1438. [CrossRef]
[51] Awogbemi O, Von Kallon DV, Kumar KS. Contributions of artificial intelligence and digitization in achieving clean and affordable energy. Intell Syst Appl 2024;22:200389. [CrossRef]
[52] Ozsari I, Ust Y, Karakurt AS. Exergetic performance analysis and comparison of oxy-combustion and conventional gas turbine power cycles. Sigma J Eng Nat Sci 2023;41:575–591.
[53] Asgharian P, Noroozian R. Modeling and model predictive control of a microturbine generation system for stand-alone operation. 2019;37:705-722.
[54] Şahin Fİ, Acarali N. Evaluation of properties for synthetic polymers in medicine. 2024;42:1315-1324.
[55] Ergüner A, Özkan R, Koca K, Genç MS. Improvement of mechanical behaviour of wind turbine blade using nanofluid-graphene and/or glass fiber in epoxy resin. Sigma J Eng Nat Sci 2021;39:58-69.
[56] Kumar KS, Palanisamy R, Aravindh S, Mohan GS. Design and analysis of windmill blades for domestic applications. Int J Mech Eng Technol 2017;8:25–36.
[57] Sunil Kumar K, Kamalakar, V, Palani S, Muniamuthu S, Belinda CM. Design of K-type propeller optimized with lightweight aluminum material and its CFD analysis for marine-based applications. In: Recent Trends Therm Fluid Sci. Singapore: Springer Nature Singapore; 2024. p. 375–390.
[58] Kumar KS, Muniamuthu S, Tharanisrisakthi BT. An investigation to estimate the maximum yielding capability of power for mini Venturi wind turbine. Ecol Eng Environ Technol 2022;23:72–78. [CrossRef]
[59] Kumar KS, Arun S, Mohan A. Identification experimental analysis of noise and vibration reduction in windmill gear box for 5MW wind turbine. Int J Mech Eng Technol 2016;7:76–85. [CrossRef]
[60] Kabak M, Taşkinöz G. Determination of the installation sites of wind power plants with spatial analysis: A model proposal. Sigma J Eng Nat Sci 2020;38:441-457.
[61] Kumar KS, Surakasi R, Mohan A, Tharanisrisakthi BT, Muniamuthu S, Geetha NB. Emerging trends and global challenges to predict drop in thermal performance of WTG gearbox. J Therm Eng 2024;10:657–669.
[62] Zhang Z. Pelton Turbines. Nee York: Springer Nature; 2016. [CrossRef]
[63] Zoppé B, Pellone C, Maitre T, Leroy P. Flow analysis inside a Pelton turbine bucket. J Turbomach 2006;128:500. [CrossRef]
[64] Nava N, Reddy I, Prasad TS. Design and static analysis of Pelton turbine bucket. Int J Sci Technol Manag 2015;4:19-25. [CrossRef]
[65] Vessaz C, Andolfatto L, Avellan F, Tournier C. Toward design optimization of a Pelton turbine runner. Struct Multidiscip Optim 2017. Preprint. doi: 10.1007/s00158-016-1465-7.
[66] Vessaz C, Jahanbakhsh E, Avellan F. Flow simulation of a Pelton bucket using finite volume particle method. IOP Conf Ser Earth Environ Sci 2014;22:012003. [CrossRef]
[67] Lakdawala H, Gupta A, Patel V, Jariwala H, Chaudhari G. Experimental investigations of jet expansion for hydraulic nozzles of different materials. Int J Eng Trends Technol 2022;70:137–142. [CrossRef]

[68] Xiao Y, Wang Z, Zhang J, Zeng C, Yan Z. Numerical and experimental analysis of the hydraulic performance of a prototype Pelton turbine. Proc Inst Mech Eng A J Power Energy 2014;228:46–55. [CrossRef]
[69] Xiao YX, Han FQ, Zhou JL, Kubota T. Numerical prediction of dynamic performance of Pelton turbine. J Hydrodyn 2007;19:356–364. [CrossRef]
[70] Alomar OR, Abd HM, Salih MMM, Ali FA. Performance analysis of Pelton turbine under different operating conditions: An experimental study. Ain Shams Eng J 2022;13:101684. [CrossRef]
[71] Syofii I, Hidayatullah AB, Adanta D, Sari DP, Burlian F, Saputra MAA. Pico scale Turgo turbine design for remote areas application using velocity triangle approach. J Adv Res Fluid Mech Therm Sci 2022;97:157–167. [CrossRef]
[72] Elgammi M, Hamad AA. A feasibility study of operating a low static pressure head micro Pelton turbine based on water hammer phenomenon. Renew Energy 2022;195:1–16. [CrossRef]
[73] Hlabanelo JM, Sob PB, Alugongo AA. A study to improve the efficiency and performance of a Pelton wheel using potential energy at low heads. Int J Eng Res Technol 2020;13:2915–2926. [CrossRef]
[74] Nigussie T, Engeda A, Dribssa E. Design, modeling, and CFD analysis of a micro hydro Pelton turbine runner: For the case of selected site in Ethiopia. Int J Rotating Mach 2017;2017:030217. [CrossRef]

Appendix 1. Uncertainty analysis for full (100 % GO) gate opening and maximum hydraulic efficiency

Nozzles with Pelton runners	Angular velocity(ω), rad/sec	Torque (T) N-m	Head (H), m	Flow rate (Q), m^3/sec	$\frac{d\eta_h}{\eta_h}$	Uncertainty (% ge)
SSN1 17 mm -CPT	96	8	43	0.00239	0.011551	1.16
SSN1 17 mm -HPT	96.85	7.34	43	0.00266	0.011482	1.15
SSN2 23 mm -CPT	111.71	7.01	43	0.00500	0.010272	1.03
SSN2 23 mm -HPT	98.94	8.83	43	0.00536	0.01126	1.13
PYN1 17 mm-CPT	106.58	8.66	43	0.00366	0.010617	1.06
PYN1 17 mm-HPT	94.54	8.75	43	0.00366	0.011685	1.17
PYN2 18 mm-CPT	105.85	8.42	43	0.00381	0.010678	1.07
PYN2 18 mm-HPT	98.1	8.17	43	0.00344	0.011348	1.13
PYN3 19 mm-CPT	100.72	8.25	43	0.00442	0.011109	1.11
PYN3 19 mm-HPT	103.13	8.13	43	0.00446	0.010904	1.09
PYN4 23 mm-CPT	96.43	9.9	43	0.00586	0.011485	1.15
PYN4 23 mm-HPT	82.19	8.33	43	0.00585	0.013146	1.31